Technical Report
**TR-19-23**
February 2020

# Probability distributions for mean sea level and storm contribution up to 2100 AD at Forsmark

**Havu Pellikka**
**Jani Särkkä**
**Milla Johansson**
**Heidi Pettersson**

SVENSK KÄRNBRÄNSLEHANTERING AB

SWEDISH NUCLEAR FUEL
AND WASTE MANAGEMENT CO

Box 3091, SE-169 03 Solna
Phone +46 8 459 84 00
skb.se

SVENSK KÄRNBRÄNSLEHANTERING

ISSN 1404-0344
**SKB TR-19-23**
ID 1874300
December 2019

# Probability distributions for mean sea level and storm contribution up to 2100 AD at Forsmark

Havu Pellikka, Jani Särkkä, Milla Johansson, Heidi Pettersson
Finnish Meteorological Institute

*Keywords:* Sea level rise, Sea level projections, Extreme sea levels, Combined probability distributions, Forsmark, The Baltic Sea.

# Preface

This report describes a study on future potential relative sea-level rise at Forsmark under different scenarios of future human carbon emissions. The study presents long-term (rise of mean sea-level) and short-term (storm surge) sea level changes, as well as individual and combined probabilities of these. Potential sea-levels and their probabilities are presented for 2050, 2080 and 2100 AD, and for the RCP emission scenarios 2.6 (low emissions), 4.5 (intermediate emissions) and 8.5 (high emissions).

The results will be used (i) for planning and construction of the geological repository for spent nuclear fuel, (ii) for planning during the operational period of the existing repository for short-lived low- and intermediate-level waste (SFR), and (iii) to describe near-future relative sea-level changes at Forsmark in SKB assessments of long term repository safety. Since the results are partially intended to be used to protect critical infrastructure, the study also focussed on high-end, albeit unlikely, sea-level rise projections up until the end of the century, i.e. a time period corresponding to the operational period of the repositories. In the report, it is noted that this type of study should be updated in a few years' time because of the rapid development within the field of future sea-level rise under global warming. In this context it should be noted that the present report replaces the two, now outdated, SKB reports TR-09-21 and R-09-06.

The study was conducted by Havu Pellikka, Jani Särkkä, Milla Johansson and Heidi Pettersson at the Finnish Meteorological Institute (FMI). Johan Liakka and Jens-Ove Näslund (SKB) assisted in the planning of the study. The study was initiated by Jens-Ove Näslund (SKB) and Heidi Pettersson (FMI).

The report manuscript was scientifically reviewed by Dr. Dewi Le Bars, Royal Netherlands Meteorological Institute (KNMI), the Netherlands, Dr. Ralf Weisse, Helmholtz-Zentrum, Geesthacht, Germany, and Dr. Tomas Almberger, SKB. Input to earlier versions of the manuscript was provided by Jens-Ove Näslund (SKB), Johan Liakka (SKB) and Christina Truedsson (Tintra konsult).

Stockholm, December 2019

*Jens-Ove Näslund*
Coordinator Climate Research Programme SKB

# Abstract

The aim of the study was to estimate extreme sea levels that could occur at the Forsmark site up to 2100 AD. The global mean sea level is projected to rise 20–290 cm during this century due to thermal expansion of seawater and melting of land-based ice. The projections have large uncertainties, mainly related to the behaviour of the Antarctic and Greenland ice sheets in a warming climate. In this study, we combined an ensemble of different global mean sea level projections into probability distributions of global mean sea level rise for three IPCC Representative Concentration Pathways: RCP2.6 (low emissions), RCP4.5 (intermediate emissions), and RCP8.5 (high emissions).

The uneven geographical distribution of the global sea level rise was taken into account when estimating the local sea level changes at Forsmark. The isostatic uplift of 67 cm/century, counteracting the sea level rise, was also included in the projections. The 1 % to 99 % ranges of the projected relative sea level change at Forsmark from 2000 to 2100 AD are –57 to +12 cm for RCP2.6, –51 to +74 cm for RCP4.5, and –38 to +166 cm for RCP8.5.

To estimate short-term sea level variations due to storm surges, a probability distribution of daily sea level maxima representative for 2000 AD was used. The distribution was based on 850 years of sea level model simulations with atmospheric forcing from the Coupled Model Intercomparison Project Phase 3 (CMIP3) climate model simulations. In 2000 AD, the storm surge level corresponding to the probability of exceedance of $10^{-5}$ events/year was 232 cm (in RH2000, the Swedish national reference height system).

To estimate the future probabilities of extreme sea level events, two methods were applied to combine the mean sea level projections with the exceedance frequency distribution of the local daily sea level maxima. In the first method, RSL change projections were added to the distribution of daily sea level maxima. In 2050 AD, for the median RSL scenario, the sea level corresponding to the probability of exceedance of $10^{-5}$ events/year ranges from 214 cm (RCP2.6) to 224 cm (RCP8.5); in 2080 AD, from 203 cm (RCP2.6) to 228 cm (RCP8.5); and in 2100 AD, from 196 cm (RCP2.6) to 234 cm (RCP8.5). For the highest RSL scenario (99.9 %), the corresponding ranges are 237–280 cm in 2050 AD; 258–367 cm in 2080 AD; and 280–449 cm in 2100 AD. In the second method, the probability distributions of the RSL change and storm surges were combined into one distribution. The resulting sea level corresponding to the probability of exceedance of $10^{-5}$ events/year for RCP8.5 is 238 cm in 2050 AD, 312 cm in 2080 AD and 405 cm in 2100 AD.

Reliable projections of future changes in regional wind and air pressure are not yet available. Therefore, the potential impact of such changes on storm surge levels is not accounted for in the present study. Wind-generated waves were not included either, thus the results of this analysis are only applicable to places sheltered from wave action.

# Sammanfattning

Målet med denna studie var att uppskatta extrema havsnivåer vid Forsmark fram till 2100 AD. Den globala havsnivån beräknas stiga 20–290 cm under detta århundrade på grund av termisk expansion av havsvatten och avsmältning av landbaserad is. Framtida havsnivåprojektioner är behäftade med stora osäkerheter, vilka framförallt är kopplade till hur inlandsisarna på Antarktis och Grönland reagerar på ett varmare klimat. I denna studie används en ensemble av olika globala havsnivåprojektioner för att beskriva sannolikhetsfördelningar av den globala havsnivåhöjningen för tre olika utsläppsscenarier från FN:s klimatpanel IPCC: RCP2.6 (låga utsläpp), RCP4.5 (medelhöga utsläpp) och RCP8.5 (höga utsläpp).

I uppskattningarna av den framtida havsnivån vid Forsmark beaktades den ojämna geografiska fördelningen av den globala havsnivåhöjningen. Även den isostatiska höjningen, som uppgår till 67 cm/århundrade och därmed motverkar den pågående havsnivåhöjningen, inkluderades i beräkningarna. Ändringen av den relativa havsnivån (relative sea level, RSL) vid Forsmark från 2000 till 2100 AD uppskattas till mellan −57 och +12 cm för RCP2.6, mellan −51 och +74 cm för RCP4.5 och mellan −38 och +166 cm för RCP8.5 för konfidensintervallet 1–99 %.

För att uppskatta den tillfälliga höjningen av havsvattenståndet vid storm (stormflod) användes sannolikhetsfördelningen av det högsta uppskattade havsvattenståndet för varje dygn, representativt för 2000 AD. Denna sannolikhetsfördelning erhölls från en 850 år lång simulering med en havsvattenståndsmodell, vilken drevs av atmosfäriska data från klimatmodellsimuleringar inom CMIP3-projektet (Coupled Model Intercomparison Project 3). Stormflodsnivån för en årlig sannolikhet på $10^{-5}$ beräknades till 232 cm.

För att uppskatta sannolikheter för framtida extrema havsnivåer användes två metoder för att kombinera framtida projektioner av medelhavsytans höjning (RSL) med frekvensfördelningen av dygnsmaxima för havsvattenstånden (stormflod). I den första metoden adderades de projekterade ändringarna i RSL till fördelningen av dygnsmaxima för havsvattenstånden. Om RSL ändras enligt dess medianuppskattning så uppgår den totala havsnivåhöjningen till mellan 214 cm (RCP2.6) och 224 cm (RCP8.5) vid 2050 AD, mellan 203 cm (RCP2.6) och 228 cm (RCP8.5) vid 2080 AD och mellan 196 cm (RCP2.6) och 234 cm (RCP8.5) vid 2100 AD för en årlig sannolikhet på $10^{-5}$. För den högsta rapporterade uppskattningen av RSL (99,9 %) är motsvarande intervaller för den totala havsnivåhöjningen 237–280 cm vid 2050 AD, 258–367 cm vid 2080 AD och 280–449 cm vid 2100 AD. I den andra metoden beräknades en ny kombinerad sannolikhetsfördelning utifrån fördelningarna för RSL och frekvensfördelningen av dygnsmaxima för havsvattenstånden. Den resulterande kombinerade havsnivån (höjning av medelhavsyta plus stormflod) under RCP8.5 uppgår till 238 cm vid 2050 AD, 312 cm vid 2080 AD och 405 cm vid 2100 AD för en årlig sannolikhet på $10^{-5}$.

Framtida regionala projektioner av förändringar i lufttryck och vind är ännu inte tillförlitliga. Därför är den potentiella påverkan av sådana förändringar på stormflodsnivåerna inte inkluderad i studien. Denna studie inkluderar inte heller våghöjd. Resultaten från denna studie kan därför endast tillämpas för platser som är skyddade från vindgenererade vågor.

# Contents

# 1 Introduction

This report describes the results of the study "Probability distributions for mean sea-level and storm contribution up to 2100 AD at Forsmark" commissioned by the Swedish Nuclear Fuel and Waste Management Company (SKB) and conducted by the Marine Research Unit of the Finnish Meteorological Institute in 2019. The aim of the project is to analyse the extreme sea levels that could occur at the Forsmark site (Figure 1-1) up to the year 2100 AD. The Forsmark site has been selected as the location for the planned repository for spent nuclear fuel and it also hosts the existing low- and intermediate-level waste repository SFR.

Extreme sea levels and their probability of occurrence in the future depend on two factors: first, how the mean sea level is expected to change over time, and second, how large the short-term variability of sea level, associated with e.g. storm events, is and to what extent it may change in the future. In this project we analyse these two factors separately and combine the resulting probability distributions into a final probability distribution of high sea level extremes.

In a long-term timescale (decades to centuries), mean sea level changes on the Baltic Sea coasts are a balance of two opposing factors: sea level rise caused by climatic warming and the isostatic uplift caused by post-glacial rebound. While the latter is a relatively well-known process proceeding at a virtually constant rate in the time scales considered here, making projections for sea level rise is a much more challenging task. Future sea level rise depends on all parts of the climate system and the way they interact – both the physical processes in the atmosphere, oceans, cryosphere, and solid earth, as well as societal changes and policies affecting the carbon emissions over the 21st century.

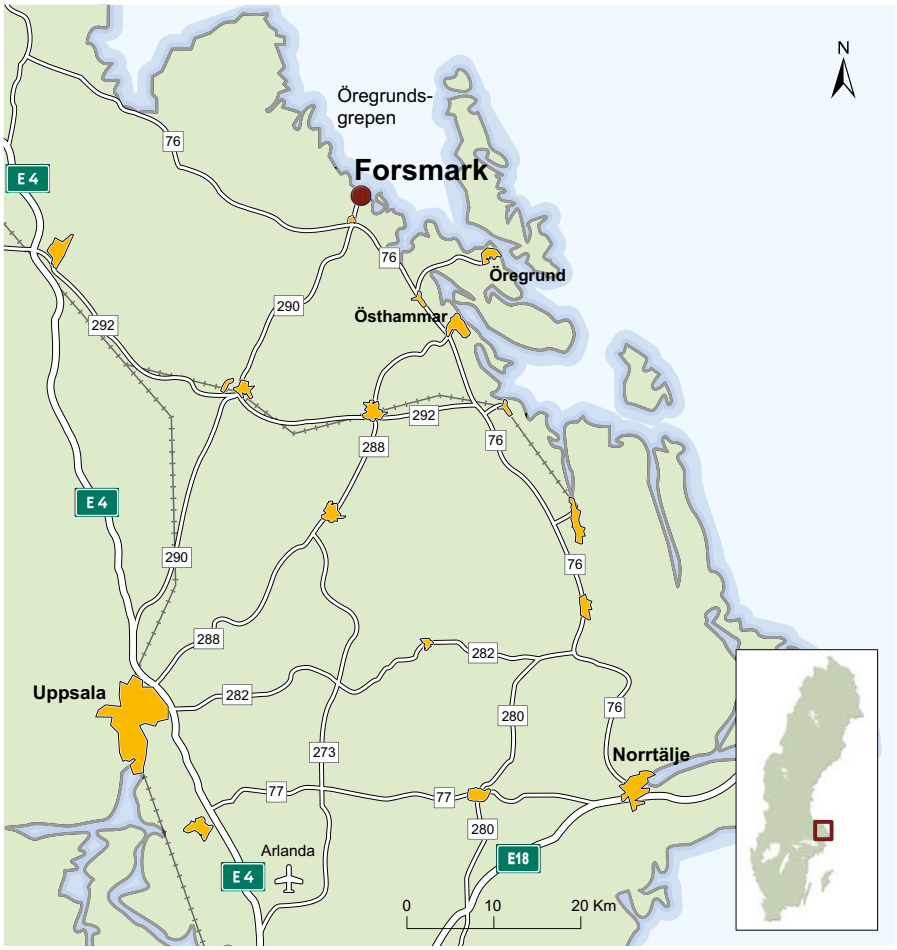


***Figure 1-1.*** *Location of the Forsmark site, Sweden, at the southwestern coast of the Gulf of Bothnia in the Baltic Sea.*

Future sea level rise is a field of active research and the science has not yet matured enough to provide consistent projections on the time scale up to 2100 AD. Complex feedback loops and processes not yet well understood, especially related to the future of the vast ice sheets of Greenland and Antarctica, result in projections with wide uncertainty limits (Church et al. 2013, DeConto and Pollard 2016, Garner et al. 2018). New projections are published regularly, and old ones are revised, often to a considerable extent. The expert elicitation study of Bamber et al. (2019) shows that uncertainty related to the ice-sheet contributions has not diminished but grown after the publication of the Fifth Assessment Report (AR5, 2013) of the Intergovernmental Panel on Climate Change (IPCC). Recently, IPCC updated their sea level projections in the Special Report on the Ocean and Cryosphere (SROCC; IPCC 2019). Compared to AR5, global mean sea level rise projections are 0.1 m higher under RCP8.5 in 2100 AD, and the likely range extends beyond 1 m due to a larger projected ice loss from the Antarctic Ice Sheet.

Due to these uncertainties, we choose an approach of using information from a wide ensemble of projections instead of a single source (Chapter 2). In this way, we hope to have a comprehensive picture of all uncertainties involved, even the unlikely ones such as the possible disintegration of the West Antarctic Ice Sheet that is not included in the present IPCC estimates. We will present this uncertainty as a probability distribution, or rather three probability distributions corresponding to three different futures of societal changes, characterized by the Representative Concentration Pathway scenarios, RCP2.6, RCP4.5, and RCP8.5 (Church et al. 2013). These emissions scenarios cover pathways from low carbon emissions (RCP2.6), through intermediate emissions (RCP4.5) up to high emissions (RCP8.5). Yet it is important to note that the results presented in this study reflect the best scientific understanding at the moment of making the assessment. These types of assessments should be updated on a regular basis in light of the most recent scientific knowledge.

By calculating separately the projections for the three RCPs, as well as calculating the scenarios for a wide range of probability levels, we aim at providing a comprehensive set of different projection options. Thus, by choosing from these, SKB can eventually decide the degree of "pessimism" they want to apply for their purposes. We aim at basing our choices of methodological details on the best scientific understanding wherever possible. However, there are cases where the choices cannot be motivated scientifically. In such cases we choose the most pessimistic option, i.e. the one allowing for the most extreme sea levels at Forsmark. The uncertainties resulting from such choices are also analysed where feasible.

As vertical movements of both sea and land surfaces are involved in sea level changes, some definitions of reference levels are necessary. In this study we use the following notations:

- **Height system RH2000** is the national Swedish height system. When sea level heights in relation to land are given for the Forsmark site in this report, the RH2000 height system is used.
- **Mean sea level (MSL)** denotes the (time-dependent) mean sea level, i.e. an average level excluding short-term variations, at a certain time instant at the study site in relation to RH2000.
- **Absolute sea level (ASL) change –** the long-term eustatic sea level change due to changes in the ocean (such as thermal expansion of seawater and water volume increase due to melting of land-based ice), which does not take into account any land movement.
- **Isostatic uplift –** the vertical movement of the Earth's crust due to postglacial rebound.
- **Relative sea level (RSL) change –** the change of mean sea level (MSL) in relation to land; RSL change = ASL change – isostatic uplift.

The short-term sea level variations (in the timescale of days) in the Baltic Sea are mainly caused by wind and air pressure variations and seiche oscillations (a standing shallow water wave in an enclosed or partially enclosed body of water), whereas the effect of tides is only a few centimetres (e.g. Witting 1911, Särkkä et al. 2017). In the timescale of weeks, the most important factor is the water volume in the Baltic Sea, which is mainly controlled by inflow and outflow of water through the Danish Straits. The most extreme sea level events are usually a result of the joint effect of these factors.

The sea level measurements at the Forsmark tide gauge started in 1975, so the length of the observed time series is less than 50 years. Such time series is too short for estimating very rare sea levels with probabilities of occurrence of e.g. $10^{-3}$ events/year or less. Our aim in simulating the short-term sea level variations with a sea level model is therefore to produce a dataset of sea levels that exceeds the length of the available tide gauge data.

The understanding of long-term climate variation is one of the key issues in climate change research and has initiated a large number of model simulations that depict climate variations for several hundreds and even thousands of years. We produce a longer dataset of sea level variations by utilizing several climate scenario simulations produced by different research institutes in the EU funded project ENSEMBLES (van der Linden and Mitchell 2009). These simulations were based on the global simulations from the third phase of the Coupled Model Intercomparison Project (CMIP3). We use six climate scenario simulations between the years 1951 and 2100 as atmospheric forcing for a sea level model, to produce 850 years of simulated sea level variations for the Baltic Sea (Chapter 3).

Some factors that might affect the exceedance frequencies of extreme sea levels are not taken into account in this analysis. Since the short-term variations are mainly caused by wind and air pressure variations, a future change in the behaviour of these atmospheric factors might change the sea level behaviour, too. Likewise, changes in wind climate might change the Baltic Sea water balance. However, projections of such changes are still highly uncertain, and there is no agreement among models on what kind of changes to expect. Thus, we ignore such changes and assume the future short-term sea level variability to be similar to the present-day variability. These factors are further discussed in Chapter 5.

On a coastline exposed to waves, the flood level is a sum of the effect of the sea level variations and the wave run-up (e.g. Leijala et al. 2018). We do not include waves in the present analysis, and the results reported here are thus applicable only to places sheltered from wave action.

# 2 Mean sea level projections

## 2.1 Ensemble of global sea level projections

We assess future changes in global mean sea level based on an ensemble of nine projections from recent scientific literature (Table 2-1). Because of large uncertainties in sea level rise projections (mainly related to the uncertain future of the Antarctic ice sheet), the upper end of the projections is poorly constrained and published estimates vary widely. Upper (95 %) estimates of sea level rise by 2100 AD range from ~ 1 m (IPCC AR5; Church et al. 2013) to ~ 3 m (Le Bars et al. 2017). Thus, we construct a probability distribution of sea level rise based on the ensemble of the selected recent projections, using a method documented in more detail in Johansson et al. (2014) and Pellikka et al. (2018).

The projections in the ensemble are based on different methods: both *process-based* projections (e.g. the methods used in the projections selected for the assessment made by IPCC 2013) and *semi-empirical* projections are included. In process-based modelling, each physical process causing sea level rise is modelled separately. In contrast, semi-empirical models are based on an empirical relationship between some climatic variable (e.g. the global mean temperature or radiative forcing) and global sea level rise. The process-based and semi-empirical methods are explained in more detail e.g. in Church et al. (2013) and Pellikka et al. (2018).

The projections are based on different methods, and there are differences in the reference periods used, which makes the projections not directly comparable. For our analysis, we normalize all projections to the common time interval 2000–2100 AD by fitting a second-order polynomial based on three constraints: initial sea level (0) at the beginning of the time series, initial rate of sea level rise, and projected sea level in 2100 AD. The initial rate of sea level rise was assumed to be 3.2 ± 0.4 mm/a (Church et al. 2013 for 1993–2010, 5–95 % range) for all projections regardless of the exact original reference period. Sea level in 2000 AD in this second-order fit is then taken as the new reference level. Both original and normalized projections are given in Table 2-1. We used the second-order polynomial (corresponding to constant acceleration) as a simple first assumption for a process that definitely is not linear but accelerating. Some of the higher projections might have a faster acceleration on the latter half of the 21st century, but detailed studies of these are beyond the scope of this analysis.

The IPCC AR5 (Church et al. 2013) gives ranges of projections which are based on the 5–95 % range of the climate models, but they assess their likelihood as “likely”, which by their definition corresponds to a 66–100 % probability. This would more appropriately translate into a 17–83 % range, to account for the uncertainty in this likelihood estimate. However, we combine the AR5 projections with eight other projections, which are based on different methods and handle uncertainties in different ways, many of them giving projections with wider probability ranges. As the AR5 projection forms only a small portion of the final distribution, we consider that this likelihood uncertainty is accounted for in our method. Thus, we apply the 5–95 % range on the IPCC AR5 projections.

We include the normalized projections of Table 2-1 to our ensemble with equal weights, thus assuming that each of them is equally plausible. This assumption can be questioned; for instance, Pellikka et al. (2018) and Johansson et al. (2014) used a lower/higher weight for certain projections due to lower/higher confidence in them. For example, Johansson et al. (2014) applied a lower weight of 0.5 (in contrast to the default 1) in cases where several papers used similar background assumptions (such as the semi-empirical projections) to compensate their large proportion in the scenario ensemble, and a weight of 2 for a scenario based on a review of several papers (the IPCC AR4; Meehl et al. 2007). However, giving equal weight reflects the fact that we cannot rule out the plausibility of any of the studies, even the highest projections. We take a closer look on the effect of weighting on the results in Section 5.1.1.

**Table 2-1. The ensemble of nine global mean sea level projections (cm) for 2100 AD (5–95 % ranges) used in the present analysis. The sea level projections have been produced using different methods, as indicated in the table. Upper values are the original projections as given in the referred publications, while lower (italicized) values are recalculated values used in this analysis. The small differences of a few centimetres come from i) normalization to the reference period 2000–2100 AD, and/or ii) recalculating the sum of different contributors to yield total sea level rise.**

| Study | Reference period | RCP2.6 | RCP4.5 | RCP8.5 | Method |
|---|---|---|---|---|---|
| **Jevrejeva et al. (2012)** | 1980–2000<br>*2000* | 36–83<br>*33–79* | 52–110<br>*49–106* | 81–165<br>*78–160* | Semi-empirical |
| **IPCC AR5 (Church et al. 2013)** | 1986–2005<br>*2000* | 28–61<br>*27–61* | 36–71<br>*34–71* | 52–98<br>*49–96* | Process-based |
| **Jevrejeva et al. (2014)/ Grinsted et al. (2015)** | 2000 | | | 45–183 | Process-based |
| **Kopp et al. (2014)** | 2000<br>*2000* | 29–82<br>*29–82* | 36–93<br>*37–93* | 52–121<br>*54–120* | Process-based |
| **Kopp et al. (2016)** | 2000 | 24–61 | 33–85 | 52–131 | Semi-empirical |
| **Mengel et al. (2016)** | 1986–2005<br>*2000* | 28–56<br>*25–52* | 37–77<br>*34–74* | 57–131<br>*52–126* | Semi-empirical |
| **Goodwin et al. (2017)** | 1986–2005<br>*2000* | 45–72<br>*44–70* | 55–84<br>*54–82* | 76–105<br>*75–103* | Process-based + semi-empirical |
| **Kopp et al. (2017)** | 2000 | 26–98 | 50–158 | 93–243 | Process-based |
| **Le Bars et al. (2017)** | 1986–2005<br>*2000* | | 37–177<br>*36–175* | 81–292<br>*80–290* | Process-based |

## 2.2 Regionalization of the global projections

As mentioned previously, sea level rise is geographically uneven. The effect of thermal expansion and ocean dynamics varies in different areas (e.g. Church et al. 2013). Sea level rise from glaciers and ice sheets is also unevenly distributed, due to changes in the gravitational field as the large ice masses melt and vertical crustal movements when the mass loading changes. The resulting distribution of sea level change is called the “fingerprint” of the ice sheet in question (Mitrovica et al. 2001).

We analyse the regional thermal expansion and ocean dynamics component in the Coupled Model Intercomparison Project 5 (CMIP5) climate models, which is the model ensemble used to construct sea level projections in IPCC AR5. As a small inland sea, the Baltic Sea is not well represented in global climate models, so these results should be considered rough estimates. According to the CMIP5 results, the regional sea level rise component in the Baltic Sea from thermal expansion and ocean dynamics is higher than the global mean by up to 27 cm (upper limit of RCP8.5, Table 2-2).

**Table 2-2. The regional thermal expansion and ocean dynamics component of sea level rise from CMIP5 models: mean over the Baltic Sea (cm, 2081–2100 AD relative to 1986–2005 AD). In comparison, the global mean thermal expansion component from IPCC AR5 (Church et al. 2013). Normalization of these values to the time interval 2000–2100 AD is carried out when this component is included in the regional projections of total sea level rise.**

| The regional thermal expansion and ocean dynamics component of sea level rise | | | | | | |
|---|---|---|---|---|---|---|
| | Mean over the Baltic Sea | | | Global mean | | |
| | mean | 5 % | 95 % | mean | 5 % | 95 % |
| **RCP2.6** | 17 | 9 | 25 | 14 | 10 | 18 |
| **RCP4.5** | 26 | 14 | 38 | 19 | 14 | 23 |
| **RCP8.5** | 43 | 25 | 60 | 27 | 21 | 33 |

Source: Regional sea level data from IPCC AR5 distributed in netCDF format by the Integrated Climate Data Center (ICDC, icdc.cen.uni-hamburg.de) University of Hamburg, Hamburg, Germany.

We estimate the regional effect of glacier and ice sheet contributions by using fingerprint coefficients from Kopp et al. (2014). At Forsmark, these are: 0.05 for Greenland (i.e. ASL rise contribution from the Greenland ice sheet in Forsmark is only 5 % of the global mean contribution from the Greenland ice sheet), 1.03 for West Antarctica (103 % of the global mean value), 1.08 for East Antarctica, and 0.25 for small glaciers and ice caps.

Some uncertainty is associated with the fact that the sea level rise projections typically give only the total Antarctic contribution and do not differentiate between East and West Antarctica. We use the fingerprint of West Antarctic Ice Sheet (1.03) to scale the Antarctic contributions, as the WAIS is considerably more sensitive to global warming and most of the Antarctic contribution over the 21st century is expected to originate from there. While some areas in East Antarctica may also be vulnerable and subject to retreat, in total the EAIS contribution is assessed to be clearly smaller over the 21st century than the WAIS contribution (Bamber et al. 2019).

Three of the projections in Table 2-1 also include information on the contributions of different sea level rise components (IPCC AR5, Kopp et al. 2014, Mengel et al. 2016). These are regionalized as follows. The global thermal expansion component is replaced with regional estimates in Table 2-2, and glacier and ice sheet components are adjusted using the coefficients above. After making the regional adjustments, we sum the contributions to obtain the total regional ASL rise. We then fit a line to the obtained pairs of global vs. regional ASL rise (blue line in Figure 2-1) and use that to scale the other global projections in the ensemble. For more details on this method, see Pellikka et al. (2018).

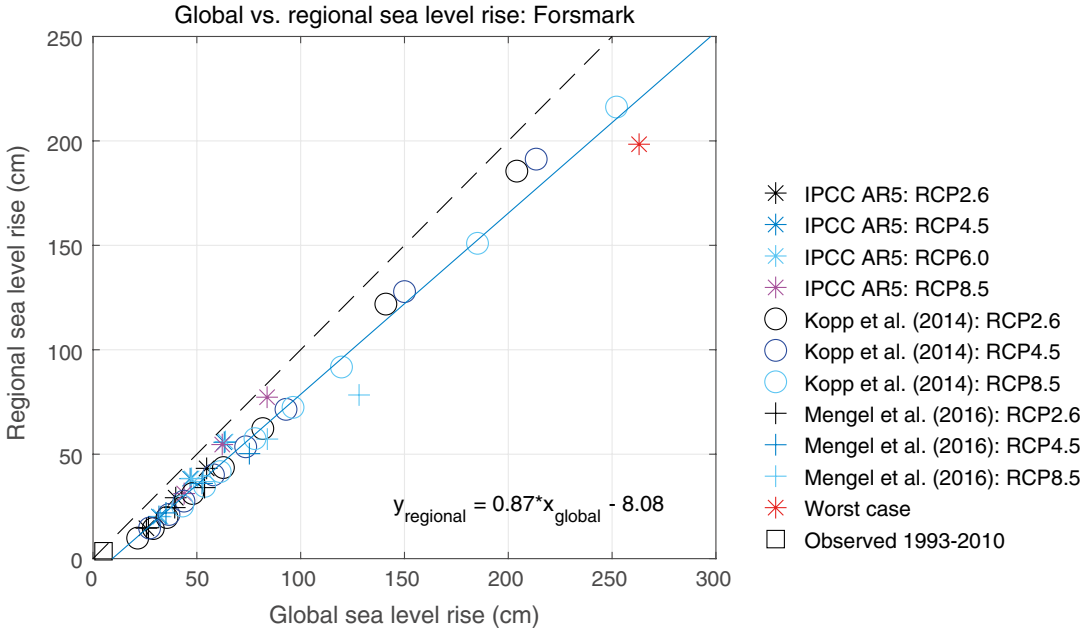


***Figure 2-1.*** *Regional ASL rise at Forsmark versus global average ASL rise. The projections consisting of different components (thermal expansion and ocean dynamics, ice sheet and glacier melting) were adjusted component-wise. The solid line is a linear fit to all points, whereas the dashed line indicates the case where regional ASL rise equals the global average ASL rise.*

## 2.3 Forming the probability distribution

Most of the projections in Table 2-1 do not provide the full probability distribution, only a few probability levels. After making the regional adjustments described in Section 2.2, we fit probability distributions to these individual projections. Most projections are not symmetrical but positively skewed, with a longer upper tail representing low-probability, high-impact scenarios such as the disintegration of the West Antarctic Ice Sheet. As the exact shape of the distribution is unknown in most cases, we test different types of distribution functions that allow a positive skew: Weibull, skewed Gaussian, and Fréchet.

Figures in Appendix 1 show the fitting of probability distributions to individual regional sea level rise projections (Forsmark, RCP8.5 as an example). It turns out that none of the distribution functions gives a good fit to all projections. Thus, we choose the type of the distribution individually for each projection (Table 2-3). There are cases where the best fit is not clearly defined; in this case we choose the most conservative, or the most pessimistic fit, i.e. the fit giving the highest probabilities for high extremes, according to the strategy outlined in Section 1. The effect of the choice of distribution function to the results is discussed in Section 5.1.2.

For each RCP emission scenario, we then sum the nine probability distributions $F_i(x)$ from individual studies to obtain the mixture distribution

$$F(x) = \frac{1}{9}\sum_{i=1}^{9} F_i(x) \qquad (2\text{-}1)$$

as the probability distribution of sea level rise at Forsmark from 2000 to 2100 AD. The ASL rise at Forsmark as a function of probability level and RCP emission scenario is given in Table 2-4.

**Table 2-3. The probability distribution functions fitted to sea level rise projections.**

| Projection | Function |
|---|---|
| **Jevrejeva et al. (2012)** | Fréchet |
| **IPCC AR5 (Church et al. 2013)** | Fréchet |
| **Jevrejeva et al. (2014)/Grinsted et al. (2015)** | No fit; the probability distribution is given in the publication |
| **Kopp et al. (2014)** | Fréchet |
| **Kopp et al. (2016)** | Fréchet |
| **Mengel et al. (2016)** | Fréchet |
| **Goodwin et al. (2017)** | Weibull |
| **Kopp et al. (2017)** | Weibull |
| **Le Bars et al. (2017)** | Weibull |

**Table 2-4. Rise in ASL (i.e. without the effect of isostatic uplift; cm) at Forsmark from 2000 to 2100 AD, based on the ensemble of sea-level projections (Table 2-1), the regionalization (Section 2.3), and fitting of distribution functions (Table 2-3).**

| The projected rise (cm) in absolute sea level ASL from 2000 to 2100 AD | | | | | | | | |
|---|---|---|---|---|---|---|---|---|
| **Emission scenario** | **Probability level** | | | | | | | |
| | 1 % | 5 % | 17 % | 50 % | 83 % | 95 % | 99 % | 99.9 % |
| **RCP2.6** | 11 | 15 | 20 | 31 | 45 | 59 | 79 | 115 |
| **RCP4.5** | 17 | 23 | 30 | 46 | 72 | 108 | 141 | 175 |
| **RCP8.5** | 29 | 37 | 48 | 69 | 116 | 179 | 233 | 285 |

## 2.4 Relative sea level (RSL) change at Forsmark up to 2100 AD

As a final step, the effect of local isostatic uplift is added to the ASL projections to obtain the RSL change at Forsmark. The present-day isostatic uplift at Forsmark (relative to the geoid) amounts to 6.7 ± 0.2 mm/year (Vestøl et al. 2019), where the uncertainty interval refers to the standard error (1 σ). This uplift rate is here assumed to be constant up to 2100 AD.

We calculate the RSL change for the intermediate years 2050 and 2080 AD by making a second-order fit to the RSL change in 2000 to 2100 AD and assuming an initial sea level rise rate of 3.2 ± 0.4 mm/a in 2000 AD (Church et al. 2013) minus the land uplift (6.7 ± 0.2 mm/a). The net effect of these (−3.5 mm/a) is similar to the observed RSL trend at Forsmark in 1989–2018 AD (Holgate et al. 2013, PSMSL 2019), after subtracting the effect of the Baltic Sea water balance (Figure 2-2). We calculated the water balance using the correlation of the annual mean sea levels with the zonal geostrophic wind over the southern Baltic Sea, see Johansson et al. (2014) for a detailed description of the method. The second-order time development (constant acceleration), is in line with the assumption of a constant acceleration of the global sea level rise made in Section 2.1. The resulting probability distributions for RSL change from 2000 to 2050 AD, 2080 AD and 2100 AD at Forsmark are shown in Figures 2-3, 2-4 and 2-5, and the RSL changes at some probability levels are listed in Table 2-5.

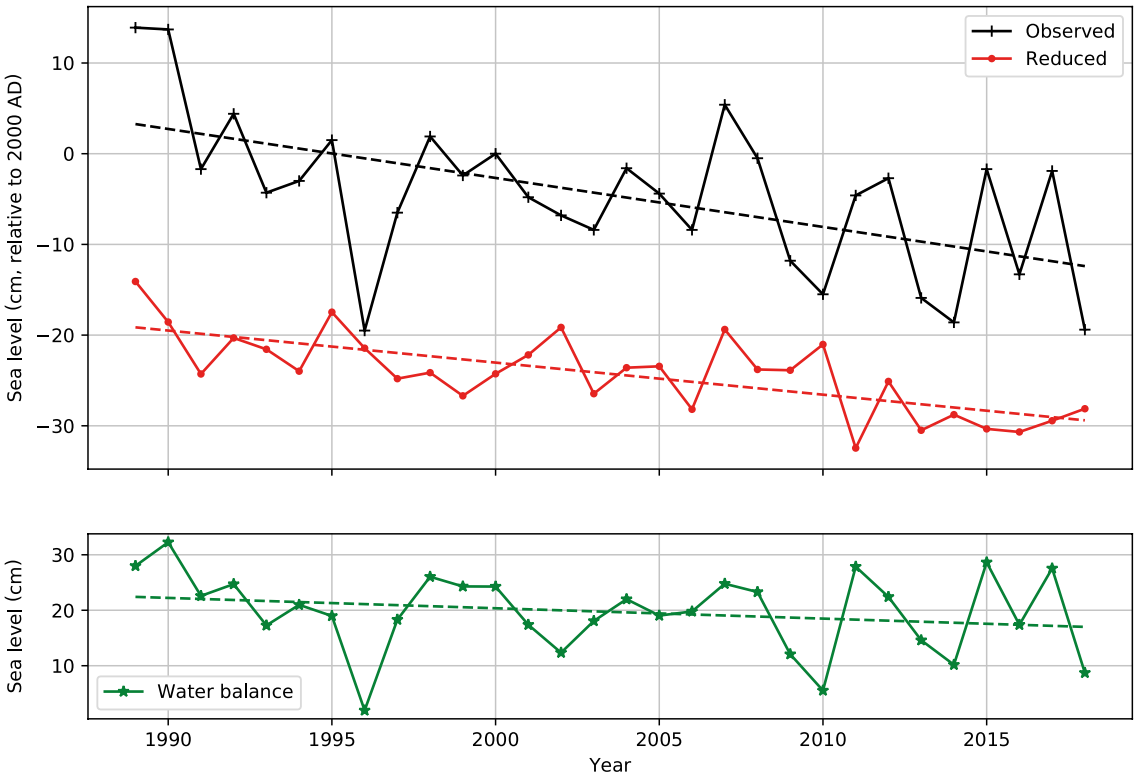


***Figure 2-2.*** *The observed annual mean relative sea level at Forsmark in 1989–2018 AD, and reduced values from which the effect of the Baltic Sea water balance has been subtracted (see text). The trend in the reduced values, −3.5 mm/a, corresponds to the net effect of the regional sea level rise and the local land uplift.*

**Table 2-5. RSL change (i.e. the net effect of ASL rise and isostatic uplift; cm) at Forsmark from 2000 to 2050, 2080 and 2100 AD.**

| Emission scenario | Year | 1 % | 5 % | 17 % | 50 % | 83 % | 95 % | 99 % | 99.9 % |
|---|---|---|---|---|---|---|---|---|---|
| **RCP2.6** | 2050 | −25 | −23 | −21 | −18 | −13 | −10 | −4 | 5 |
| | 2080 | −43 | −40 | −36 | −29 | −19 | −10 | 3 | 26 |
| | 2100 | −57 | −53 | −48 | −36 | −22 | −8 | 12 | 48 |
| **RCP4.5** | 2050 | −23 | −21 | −19 | −14 | −7 | 3 | 11 | 20 |
| | 2080 | −39 | −35 | −30 | −19 | −2 | 21 | 43 | 65 |
| | 2100 | −51 | −44 | −37 | −21 | 5 | 41 | 74 | 107 |
| **RCP8.5** | 2050 | −20 | −17 | −14 | −8 | 4 | 20 | 34 | 48 |
| | 2080 | −31 | −25 | −18 | −4 | 26 | 66 | 101 | 135 |
| | 2100 | −38 | −29 | −19 | 2 | 49 | 111 | 166 | 217 |

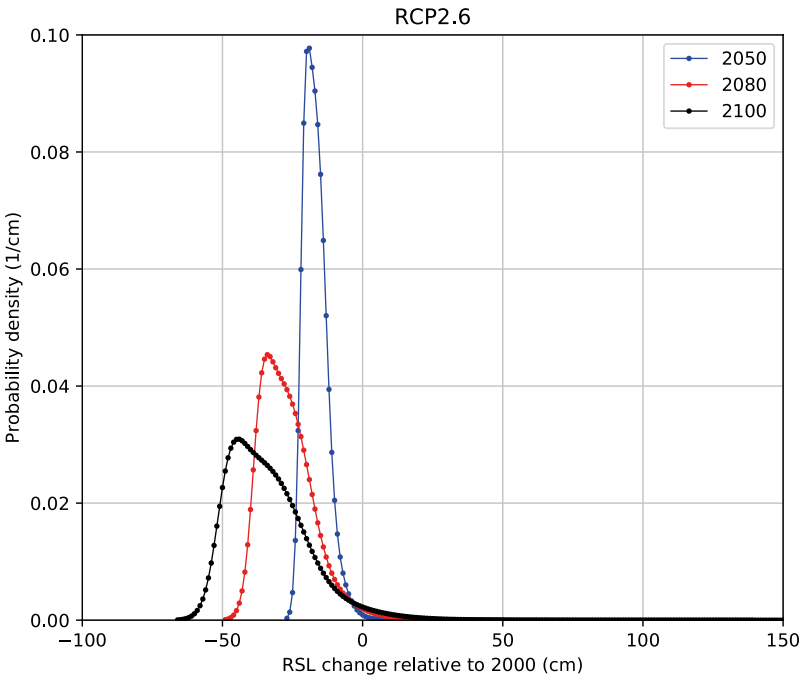


***Figure 2-3.*** *Probability density functions for the relative sea level change (cm) from 2000 to 2050, 2080 and 2100 AD at Forsmark under the IPCC emission scenario RCP2.6.*

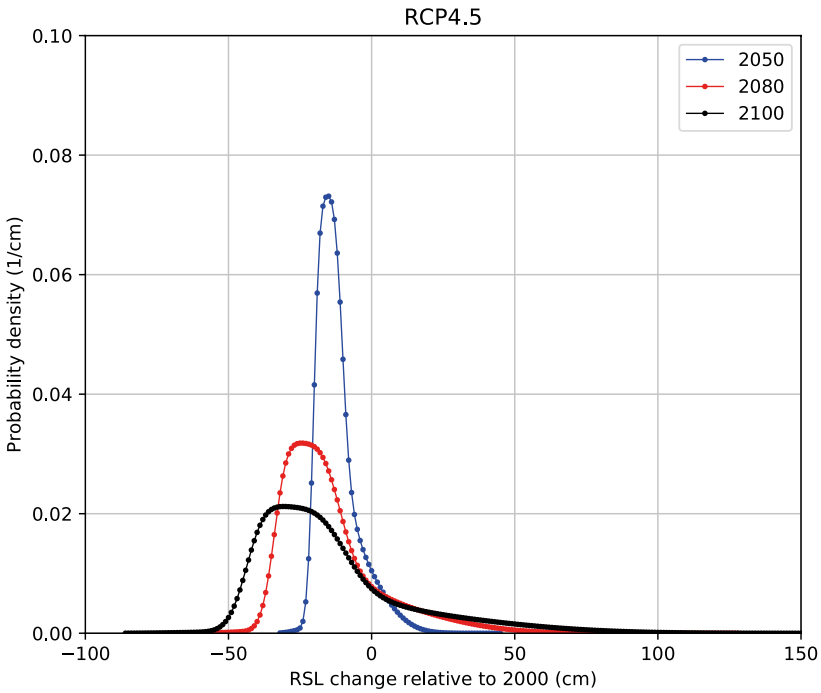


***Figure 2-4.*** *Probability density functions for the relative sea level change (cm) from 2000 to 2050, 2080 and 2100 AD at Forsmark under the IPCC emission scenario RCP4.5.*

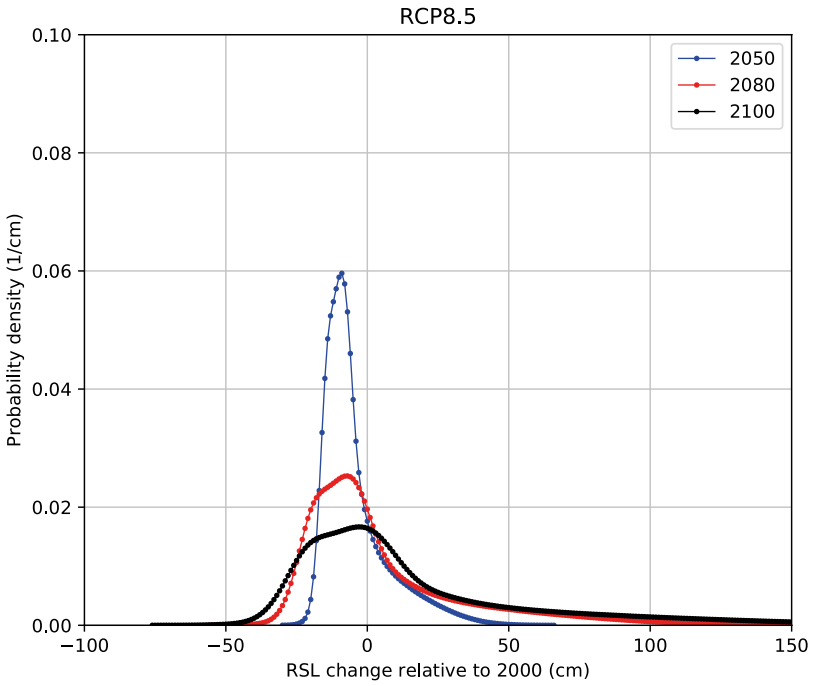


***Figure 2-5.*** *Probability density functions for the relative sea level change (cm) from 2000 to 2050, 2080 and 2100 AD at Forsmark under the IPCC emission scenario RCP8.5.*

# 3 Short-term sea level variation in 2000 AD

## 3.1 Model description

We produce the 850-year dataset of simulated short-term sea level variations for the Baltic Sea with a sea level model, using six regional climate model simulations between 1951 and 2100 AD as atmospheric forcing. The climate simulations are from the third phase of the Coupled Model Intercomparison Project (CMIP3), produced by different research institutes in the ENSEMBLES project (van der Linden and Mitchell 2009). The details of the simulations are given in Table 3-1.

In the regionalized CMIP3 scenarios, changes in windiness are small within the simulation period. A recent study (Ruosteenoja et al. 2019) showed no increase in windiness in the CMIP5 scenarios either. We use the CMIP3 scenarios in describing the present-day climate variability, as there were no regionalised scenarios for CMIP5 available, even though CMIP5 was used for the analysis of the future mean sea level rise (Chapter 2).

**Table 3-1. The CMIP3 climate simulations used as atmospheric forcing for the sea level model.**

| Institute | Time range | Time resolution | Global climate model | Regional climate model |
|---|---|---|---|---|
| **C4I (Ireland)** | 1951–2100 | 6H | HadCM3Q16 | RCA3 |
| **ETHZ (Switzerland)** | 1951–2100 | 3H | HadCM3Q0 | CLM |
| **MPI (Germany)** | 1951–2080 | 6H | ECHAM5 | MPI-M-REMO |
| **KNMI (Netherlands)** | 1951–2100 | 3H | ECHAM5r3 | RACMO2 |
| **SMHI (Sweden)** | 1961–2100 | 3H | BCM | RCA |
| **SMHI (Sweden)** | 1961–2100 | 3H | HadCM3Q3 | RCA |

The sea level simulations are performed using a multi-component sea level model (hereafter denoted "sea level model" for simplicity) consisting of numerical and statistical components, which are separately modelled. Separating the components allows for faster calculations than with a full 3D ocean circulation model without reducing the accuracy of the model (Meier et al. 2004, Särkkä et al. 2017). The correlations between tide gauge observations and simulated sea levels are above 0.9 and rms error of the order of 10 cm (Särkkä et al. 2017). Here a brief description of the components is given, whereas a more detailed description is given in Särkkä et al. (2017).

**The first model component** describes the sub-weekly variation of sea level caused mainly by winds, air pressure and seiche oscillation, treating the Baltic Sea as a closed basin. The numerical sea-level model used (Häkkinen 1980) is based on a model developed by Hansen (1956). This component has hourly temporal resolution.

**The second model component** describes the variation of the Baltic Sea average level (i.e. total water volume, or water balance) due to the water exchange between the Baltic Sea and the North Sea through the Danish Straits. Johansson et al. (2014) and Johansson and Kahma (2016) showed that about 80 % of this variation can be described with a statistical correlation with the zonal geostrophic wind speed (calculated from the mean-sea-level air pressure gradient) at the location 55 °N, 15 °E (in the southern Baltic Sea, over the Bornholm island). This variation is thus modelled statistically using zonal winds at 55 °N, 15 °E.

As there is a correlation between daily averages of the zonal wind in Bornholm and hourly sea level values, we express the water balance component $h_{WB}(t)$ as a function of the regression coefficients $a(T)$ and the zonal Bornholm winds $v_B(t)$ of the preceding 65 days as

$$h_{WB}(t) = \sum_{T=1}^{65} a(T) v_B(t - T), \quad (3\text{-}1)$$

where $t$ is time in days and $T$ is difference in days between the Bornholm wind and sea level (Särkkä et al. 2017). The temporal resolution of this component is 24 hours. The $h_{WB}$ values are interpolated linearly to hourly resolution to enable summing the different model components in hourly resolution. The

regression coefficients were calculated from coefficients for the Finnish tide gauges (the list of the tide gauges can be found in Särkkä et al. 2017) by applying Fourier transformation. The coefficients for all the tide gauges are very similar, thus the coefficients in Equation (3-1) can be regarded as independent of the tide gauge location. Since we calculate the total water volume in the Baltic Sea, the regression coefficients can be used with sufficient accuracy along the Swedish coast as well. We use tide gauge sea level data from years 1961–2000 AD. ERA-40 reanalysis data are used to calculate both the zonal wind at Bornholm $v_B$ and the intra-basin sea level component.

The climate scenarios used disagree on the possible changes in windiness or wind field patterns in the future (see the discussion in Section 5.2). However, in general the changes in wind climate, which affect both the first and second model components, were small in all six climate scenarios. Hence, we regard the sea level simulated using the sea level model as statistical sampling of the sea level in 2000 AD repeated 850 times. The simulated sea levels can thus be considered a stationary time series. This enables us to estimate the frequency of extreme sea levels in 2000 AD to the level of 1/850 events per year.

**The third model component** is the tide. At Forsmark, the tidal amplitude is calculated to be 4 cm at its largest, so its effect on the total sea level is very small. However, tides are included in the model simulation.

**The fourth and fifth model components** are the isostatic uplift and ASL rise, which together form the RSL change. In this study, we account for these components by using the RSL projections from Section 2.4, to be combined with the probability distribution of the short-term variability consisting of the first, second and third model components (Chapter 4). The RSL projections describe the change of the MSL from 2000 AD to 2100 AD. The MSL in the model in 2000 AD at Forsmark is adjusted by a bias correction (−1.8 cm) to correspond to the average of the observations at Forsmark (19.3 cm in 2000 AD, RH2000).

## 3.2 Probability distribution for the short-term variability

The time step of the sea level simulation was one hour. The performance of the sea level model was studied by using both ERA-40 reanalysis data 1961–2000 AD (Uppala et al. 2005) and ERA-Interim reanalysis data 1979–2012 AD (Dee et al. 2011) as atmospheric forcing. At Forsmark, the correlation is 0.92, and the root mean square error is 9 cm. The probability distribution of short-term sea level variability is formed using the daily maxima of the 850-year sea level simulation.

The differences between the simulated and observed sea levels originate both from the sea level model and from the downscaling of the global climate models to obtain the regional climate model results. In addition, the climate models themselves also have uncertainties.

The different regional climate models used in the simulations cause varying errors. The largest error comes from the RACMO2 model (Särkkä et al. 2017). The error of this model simulation is chosen to represent the error distribution of the sea level model simulation. It is calculated from the daily maxima of errors (observations minus simulations). The error distribution is extrapolated with an exponential function (black line in Figure 3-1). To reduce the effect the errors of the simulated sea level maxima have on the sea level distribution, the error distribution is combined statistically with the short-term sea level distribution using convolution. The combined distribution of the sum of the sea level and its error (black line in Figure 3-2) agrees well with the observed sea level distribution from 1983 to 2012 AD (red dots in Figure 3-2) and the distribution of simulated sea levels using ERA-Interim atmospheric forcing from 1983 to 2012 AD (cyan dots in Figure 3-2).

The estimation of exceedance frequencies lower than 1/850 per year requires extrapolation of the frequency distribution acquired from the 850-year sea level simulation (dashed black line in Figure 3-2). This is done using exponential distribution. The extrapolation function is chosen so that the probability distribution curve becomes continuous. Since the consecutive daily and monthly sea level maxima are correlated in the Baltic Sea, annual maxima should be used if one wants to use the generalized extreme value (GEV) method in the analysis: the method requires that the extremes are independent and random (Coles 2001). The shape of the distribution of the simulated annual maxima of the 850-year simulation differs significantly from the distribution of the observed annual maxima from 1983 to 2012 AD (see Figure 3-3), and the extrapolation with the GEV method would result in a curve that has a downward

bending slope. The choice of the exponential function for the extrapolation means that the extrapolated curve continues with the same slope as the existing data. In Särkkä et al. (2017), the short-term variability distribution was extrapolated with the Weibull distribution, which is very close to an exponential distribution at Helsinki up to exceedance frequency of $10^{-4}$ events/year (see Figure 11 in Särkkä et al. 2017).

The simulated sea level distribution in 2000 AD is shown as black line in Figure 3-2 and the exceedance frequencies are given in Table 3-2.

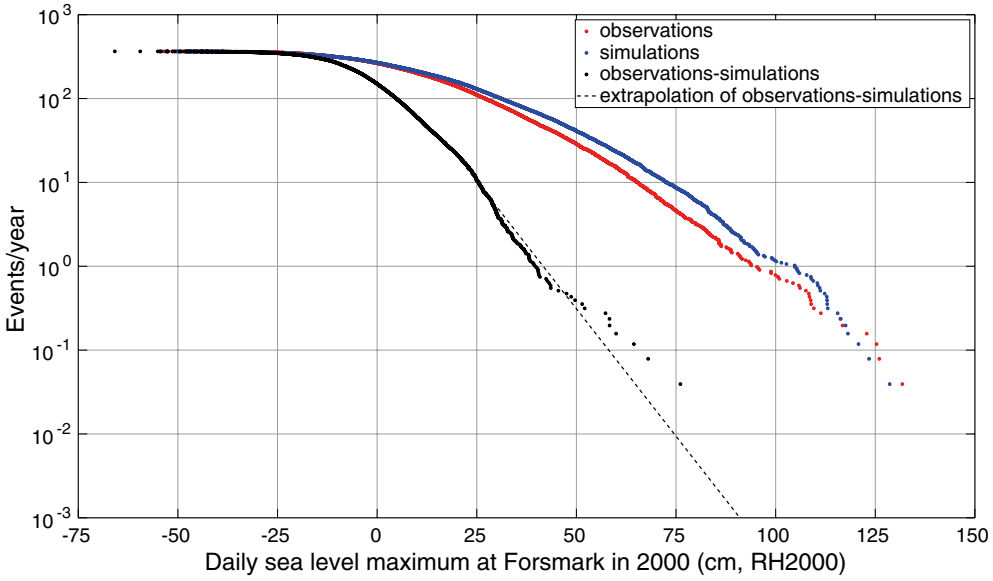


***Figure 3-1.*** *The distribution of the daily maxima of errors (black), extrapolated with an exponential function. It is the distribution of the differences of the observed (red) and simulated (blue) daily sea level maxima at Forsmark 1975–2000 AD. We used model simulations with ERA-40 reanalysis forcing, downscaled with RACMO2 regional climate model (having the largest error, see text for details).*

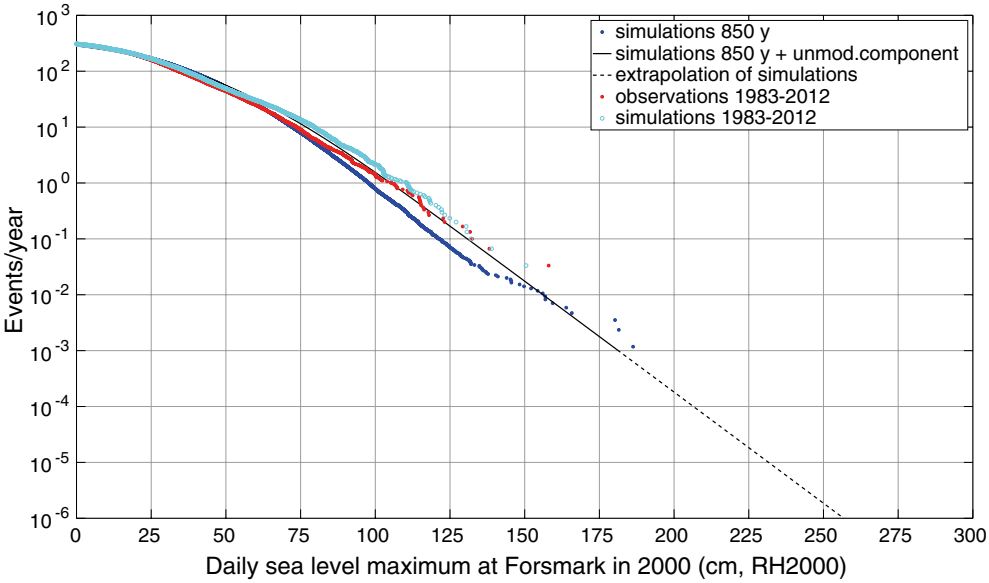


***Figure 3-2.*** *Exceedance frequency distributions of the daily sea level maxima of the combined sea level simulation forced with 6 regional climate model simulations covering 850 years. Blue = model simulation, red dots = observations 1983–2012 AD, cyan = model simulation 1983–2012 AD based on ERA-Interim reanalysis forcing, black = model simulation + model error (obtained from the analysis shown in Figure 3-1).*

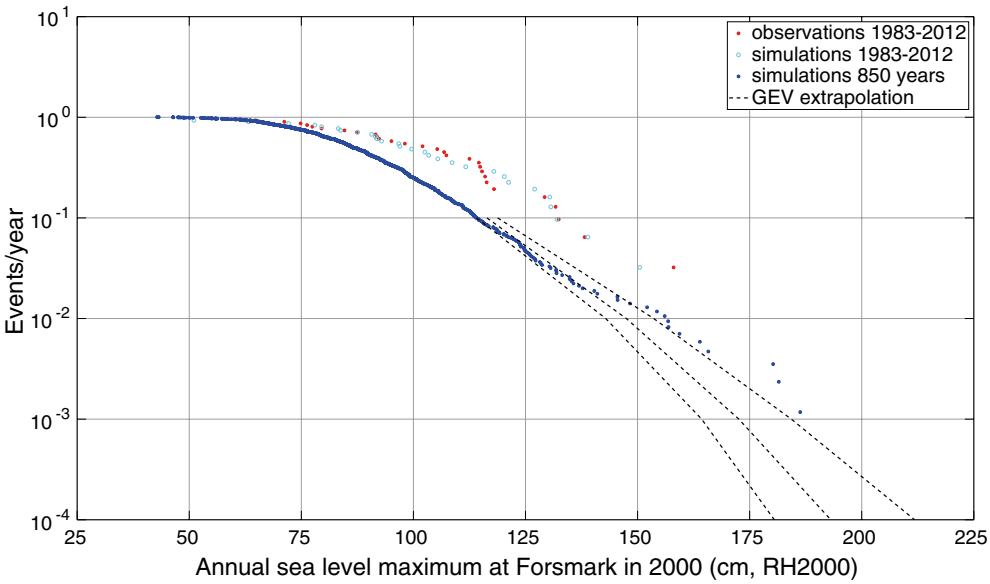


***Figure 3-3.*** *Annual sea level maxima at Forsmark from the 850-year simulation (blue) with an extrapolation with a GEV fit with 95 % confidence limits (dashed), from observations 1983–2012 AD (red) and from the ERA-Interim-based simulation 1983–2012 AD (cyan).*

**Table 3-2. Sea level estimates for selected exceedance frequencies (events/year) from the daily maxima of the 850-year simulation of the combined sea level model in 2000 AD at Forsmark (RH2000, Figure 3-2).**

| Events/year | Sea level estimates in 2000 AD (cm, RH2000) |
|---|---|
| 1 | 105 |
| 0.1 | 131 |
| 0.01 | 156 |
| $10^{-3}$ | 181 |
| $10^{-4}$ | 206 |
| $10^{-5}$ | 232 |

# 4 Combination of short-term sea level variations and RSL change for 2050, 2080 and 2100 AD

## 4.1 Exceedance frequencies of extremes in the future with selected RSL changes

In the previous chapter, the distribution of the simulated short-term sea levels was combined statistically with the error distribution to yield the probability distribution of the daily maxima, whereas the probability distributions for the RSL changes until 2050, 2080, and 2100 AD were determined in Chapter 2.

We first assess the exceedance frequencies of daily sea level maxima in the future by adding a selected RSL change (e.g., median (50 %) of the RSL change from 2000 to 2100 AD for RCP8.5; +2 cm from Table 2-5) to the exceedance frequency distribution of the daily maxima in 2000 AD, to get the exceedance frequency distribution in 2100 AD. Such distribution, which is thus based only on a shift of the distribution of the daily maxima due to the change of the RSL, describes what the exceedance frequencies would be in the year 2100 AD, provided that the corresponding RSL projection (e.g. the RCP8.5 median) were realized. The distributions do not account for any interaction between the RSL change and short-term variability, such as e.g. the dependence of surge behaviour on water depth.

These distributions are calculated for 2050, 2080 and 2100 AD; for each of the three RCP emission scenarios; and for RSL changes corresponding to the 50 %, 83 %, 95 %, 99 % and 99.9 % cumulative probability levels. The results are given in Tables 4-1 to 4-3, and plots of the exceedance frequency distributions for each year and RCP shown in Appendix 2.

**Table 4-1. Sea levels (cm, RH2000) corresponding to different exceedance frequencies at Forsmark in 2050 AD for the RCP2.6, RCP4.5 and RCP8.5 emission scenarios, assuming certain probability levels of the RSL change projection (50 %, 83 %, 95 %, 99 % and 99.9 %).**

| RCP2.6 | | | | | |
|---|---|---|---|---|---|
| **Exceedance frequency (events/year)** | **RSL projection probability level** | | | | |
| | **50 %** | **83 %** | **95 %** | **99 %** | **99.9 %** |
| 1 | 87 | 92 | 95 | 101 | 110 |
| 0.1 | 113 | 118 | 121 | 127 | 136 |
| 0.01 | 138 | 143 | 146 | 152 | 161 |
| $10^{-3}$ | 163 | 168 | 171 | 177 | 186 |
| $10^{-4}$ | 188 | 193 | 196 | 202 | 211 |
| $10^{-5}$ | 214 | 219 | 222 | 228 | 237 |
| **RCP4.5** | | | | | |
| **Exceedance frequency (events/year)** | **RSL projection probability level** | | | | |
| | **50 %** | **83 %** | **95 %** | **99 %** | **99.9 %** |
| 1 | 91 | 98 | 108 | 116 | 125 |
| 0.1 | 117 | 124 | 134 | 142 | 151 |
| 0.01 | 142 | 149 | 159 | 167 | 176 |
| $10^{-3}$ | 167 | 174 | 184 | 192 | 201 |
| $10^{-4}$ | 192 | 199 | 209 | 217 | 226 |
| $10^{-5}$ | 218 | 225 | 235 | 243 | 252 |
| **RCP8.5** | | | | | |
| **Exceedance frequency (events/year)** | **RSL projection probability level** | | | | |
| | **50 %** | **83 %** | **95 %** | **99 %** | **99.9 %** |
| 1 | 97 | 109 | 125 | 139 | 153 |
| 0.1 | 123 | 135 | 151 | 165 | 179 |
| 0.01 | 148 | 160 | 176 | 190 | 204 |
| $10^{-3}$ | 173 | 185 | 201 | 215 | 229 |
| $10^{-4}$ | 198 | 210 | 226 | 240 | 254 |
| $10^{-5}$ | 224 | 236 | 252 | 266 | 280 |

**Table 4-2. Sea levels (cm, RH2000) corresponding to different exceedance frequencies at Forsmark in 2080 AD for the RCP2.6, RCP4.5 and RCP8.5 emission scenarios, assuming certain probability levels of the RSL change projection (50 %, 83 %, 95 %, 99 % and 99.9 %).**

**RCP2.6**

| Exceedance frequency (events/year) | RSL projection probability level | | | | |
|---|---|---|---|---|---|
| | 50 % | 83 % | 95 % | 99 % | 99.9 % |
| 1 | 76 | 86 | 95 | 108 | 131 |
| 0.1 | 102 | 112 | 121 | 134 | 157 |
| 0.01 | 127 | 137 | 146 | 159 | 182 |
| $10^{-3}$ | 152 | 162 | 171 | 184 | 207 |
| $10^{-4}$ | 177 | 187 | 196 | 209 | 232 |
| $10^{-5}$ | 203 | 213 | 222 | 235 | 258 |

**RCP4.5**

| Exceedance frequency (events/year) | RSL projection probability level | | | | |
|---|---|---|---|---|---|
| | 50 % | 83 % | 95 % | 99 % | 99.9 % |
| 1 | 86 | 103 | 126 | 148 | 170 |
| 0.1 | 112 | 129 | 152 | 174 | 196 |
| 0.01 | 137 | 154 | 177 | 199 | 221 |
| $10^{-3}$ | 162 | 179 | 202 | 224 | 246 |
| $10^{-4}$ | 187 | 204 | 227 | 249 | 271 |
| $10^{-5}$ | 213 | 230 | 253 | 275 | 297 |

**RCP8.5**

| Exceedance frequency (events/year) | RSL projection probability level | | | | |
|---|---|---|---|---|---|
| | 50 % | 83 % | 95 % | 99 % | 99.9 % |
| 1 | 101 | 131 | 171 | 206 | 240 |
| 0.1 | 127 | 157 | 197 | 232 | 266 |
| 0.01 | 152 | 182 | 222 | 257 | 291 |
| $10^{-3}$ | 177 | 207 | 247 | 282 | 316 |
| $10^{-4}$ | 202 | 232 | 272 | 307 | 341 |
| $10^{-5}$ | 228 | 258 | 298 | 333 | 367 |

**Table 4-3. Sea levels (cm, RH2000) corresponding to different exceedance frequencies at Forsmark in 2100 AD for the RCP2.6, RCP4.5 and RCP8.5 emission scenarios, assuming certain probability levels of the RSL change projection (50 %, 83 %, 95 %, 99 % and 99.9 %).**

| RCP2.6 | | | | | |
|---|---|---|---|---|---|
| **Exceedance frequency (events/year)** | **RSL projection probability level** | | | | |
| | **50 %** | **83 %** | **95 %** | **99 %** | **99.9 %** |
| 1 | 69 | 83 | 97 | 117 | 153 |
| 0.1 | 95 | 109 | 123 | 143 | 179 |
| 0.01 | 120 | 134 | 148 | 168 | 204 |
| $10^{-3}$ | 145 | 159 | 173 | 193 | 229 |
| $10^{-4}$ | 170 | 184 | 198 | 218 | 254 |
| $10^{-5}$ | 196 | 210 | 224 | 244 | 280 |
| **RCP4.5** | | | | | |
| **Exceedance frequency (events/year)** | **RSL projection probability level** | | | | |
| | **50 %** | **83 %** | **95 %** | **99 %** | **99.9 %** |
| 1 | 84 | 110 | 146 | 179 | 213 |
| 0.1 | 110 | 136 | 172 | 205 | 239 |
| 0.01 | 135 | 161 | 197 | 230 | 264 |
| $10^{-3}$ | 160 | 186 | 222 | 255 | 289 |
| $10^{-4}$ | 185 | 211 | 247 | 280 | 314 |
| $10^{-5}$ | 211 | 237 | 273 | 306 | 340 |
| **RCP8.5** | | | | | |
| **Exceedance frequency (events/year)** | **RSL projection probability level** | | | | |
| | **50 %** | **83 %** | **95 %** | **99 %** | **99.9 %** |
| 1 | 107 | 154 | 216 | 271 | 322 |
| 0.1 | 133 | 180 | 242 | 297 | 348 |
| 0.01 | 158 | 205 | 267 | 322 | 373 |
| $10^{-3}$ | 183 | 230 | 292 | 347 | 398 |
| $10^{-4}$ | 208 | 255 | 317 | 372 | 423 |
| $10^{-5}$ | 234 | 281 | 343 | 398 | 449 |

## 4.2 Combined probability distributions of short-term variability and RSL change

An alternative to the method used in Section 4.1 is to combine the short-term distribution with the probability distribution of the mean sea level change by calculating the distribution of the sum of these under the assumption that the two variables are independent (convolution). These results describe the probabilities of high sea level due to storm surges and mean sea level rise combined, giving the compound risk of having a certain sea level in 2100 AD. This differs from the results in Section 4.1, which give the probability distributions of daily maxima in 2100 AD assuming the realisation of selected RSL projections (different probability levels).

We denote the total daily sea level maximum in year $N$ with $z = x + y$, where $x$ is the mean sea level change from 2000 AD to year $N$ and $y$ is the short-term daily sea level maximum in 2000 AD. The short-term sea level variation and MSL rise are assumed to be independent random variables. The cumulative distribution $F(z)$ of the sum $z = x + y$ can then be calculated using formula

$$F(z) = \int_{-\infty}^{\infty} f_x(x) F_y(z - x) dx \quad (4\text{-}1)$$

where $f_x$ is the probability density distribution of the mean sea level rise and $F_y$ is the cumulative probability distribution of short-term sea level variation. The total sea level rise distribution is thus a convolution of the mean sea level rise distribution and the short-term sea level distribution.

The short-term sea level distribution is obtained from the 850-year sea level simulation (Chapter 3), and mean sea level rise distribution from the combination of different studies of mean sea level rise (Chapter 2). For a comprehensive explanation of calculating the probability of the sum of two independent random variables, see Section 4.4 in Leijala et al. (2018).

Sea levels corresponding to certain probability levels (exceedance) at 2050, 2080 and 2100 AD, obtained from the combined distributions, are given in Tables 4-4, 4-5 and 4-6 for RCP2.6, RCP4.5 and RCP8.5, respectively, and plots of the combined distributions are shown in Appendix 2. We note that the behaviour of the combined distributions for 2100 AD is somewhat inconsistent in the high-end tail: the lowest emission scenario RCP2.6 gives higher results than RCP4.5 at the low probability range ($10^{-3}$ and smaller). We have lower confidence in the high-end tail of the combined distribution of RCP2.6 and RCP4.5 compared to RCP8.5, and these results are therefore given within brackets in Tables 4-4 and 4-5. The reasons for the lower confidence are discussed in Section 5.3.2.

**Table 4-4. Sea levels (RH2000) corresponding to different probabilities of exceedance at Forsmark in 2050, 2080 and 2100 AD, for the RCP2.6 emission scenario, obtained from the combined probability distribution of the RSL projection and the short-term variability. Results of low confidence are given within brackets; see text for discussion.**

| RCP2.6 (events/year) | 2050 (cm) | 2080 (cm) | 2100 (cm) |
|---|---|---|---|
| 1 | 89 | 84 | 87 |
| 0.1 | 115 | 114 | 128 |
| 0.01 | 140 | 148 | 196 |
| $10^{-3}$ | (166) | (183) | (253) |
| $10^{-4}$ | (191) | (214) | (289) |
| $10^{-5}$ | (216) | (240) | (317) |

**Table 4-5. Sea levels (RH2000) corresponding to different probabilities of exceedance at Forsmark in 2050, 2080 and 2100 AD, for the RCP4.5 emission scenario, obtained from the combined probability distribution of the RSL projection and the short-term variability. Results of low confidence are given within brackets; see text for discussion.**

| RCP4.5 (events/year) | 2050 (cm) | 2080 (cm) | 2100 (cm) |
|---|---|---|---|
| 1 | 96 | 111 | 139 |
| 0.1 | 122 | 142 | 177 |
| 0.01 | 147 | 169 | 212 |
| $10^{-3}$ | (173) | (196) | (246) |
| $10^{-4}$ | (198) | (222) | (277) |
| $10^{-5}$ | (223) | (247) | (304) |

**Table 4-6. Sea levels (RH2000) corresponding to different probabilities of exceedance at Forsmark in 2050, 2080 and 2100 AD, for the RCP8.5 emission scenario, obtained from the combined probability distribution of the RSL projection and the short-term variability.**

| RCP8.5 (events/year) | 2050 (cm) | 2080 (cm) | 2100 (cm) |
|---|---|---|---|
| 1 | 109 | 166 | 234 |
| 0.1 | 136 | 203 | 283 |
| 0.01 | 162 | 234 | 321 |
| $10^{-3}$ | 187 | 261 | 352 |
| $10^{-4}$ | 213 | 287 | 379 |
| $10^{-5}$ | 238 | 312 | 405 |

# 5 Discussion

## 5.1 Mean sea level projections: effect of subjective choices

### 5.1.1 Projection ensemble and weighting

The choice of the published projections that are included in our projection ensemble is somewhat subjective. The IPCC AR5 projections (Church et al. 2013) have been criticized of being potentially underestimated, as they excluded the possibility of larger sea level rise resulting from the collapse of the West Antarctic Ice Sheet (e.g. Garner et al. 2018). The IPCC SROCC was published in autumn 2019. We choose not to replace the AR5 projections with the slightly higher SROCC projections, as the potential for a larger ice loss from the Antarctic is already well accounted for in the other projections included in our ensemble.

The projections of Kopp et al. (2017) and Le Bars et al. (2017) build on the results of DeConto and Pollard (2016), projecting a large sea level rise from the Antarctic ice sheet (up to more than 1 m over the 21st century). Including these two projections in our scenario ensemble practically gives a probability of 2/9 for such high projections, which may be viewed as a rather pessimistic choice. In order not to ignore this deep uncertainty, we analyse the sensitivity of our projections for the inclusion or exclusion of these high projections.

While it has long been known that marine ice sheets are vulnerable to an adverse feedback loop once their retreat is triggered (the marine ice sheet instability or MISI hypothesis), the modelling study of DeConto and Pollard (2016) took into account some previously neglected physical processes regarding the dynamics of vertical ice cliffs. The Antarctic coastline is fringed by large floating ice shelves that buttress the flow of ice and have a stabilizing effect on the grounded part of the ice sheet. The marine ice cliff instability (MICI) hypothesis suggests that the vertical ice cliffs created by the disintegration of the ice shelves could collapse rapidly, causing a significant additional contribution to sea level rise. At the time of writing, the hypothesis is controversial and under debate in the scientific community (e.g. Edwards et al. 2019). In addition, Edwards et al. (2019) argue that the interpretation made by Le Bars et al. (2017) about the shape of the probability distribution of the Antarctic contribution leads to an overestimate of total global mean sea level rise.

Because of the uncertainty related to these studies, we test the consequences of excluding IPCC AR5, Kopp et al. (2017), and Le Bars et al. (2017) on our results. It turns out that including or excluding IPCC AR5 in the projection ensemble has a minor effect of only a few centimetres. This is to be expected, since the IPCC projection lies at the lower end of the ensemble where there are also many other projections covering this range. On the other hand, including or excluding Le Bars et al. (2017) and Kopp et al. (2017) in the ensemble has a major effect on the tail of the distribution, even several tens of centimetres (Table 5-1). This is also not surprising, since Le Bars et al. (2017) and Kopp et al. (2017) are the highest members of the ensemble and strongly influence the shape of the tail especially at the very extreme end (the 99 % and 99.9 % percentiles).

Instead of either excluding these high projections from the ensemble (giving them a weight of zero), or including them with the full weight of one, they can be given lower weights when summing the projections, see Pellikka et al. (2018) and Johansson et al. (2014). We test the effect of this by applying weights between zero and one to the projections of Le Bars et al. (2017) and Kopp et al. (2017). The results are presented in Table 5-1 and Figure 5-1. The weighting mainly affects the high end of the probability distribution, where the ASL rise increases with increasing weight of these studies. The intermediate weights between zero and one produce results that are between those obtained by completely excluding these projections or including them with the full weight.

In the final results presented in the present study, we decide to fully include Kopp et al. (2017) and Le Bars et al. (2017) in our projection ensemble (i.e. giving them a weight of one). Even Edwards et al. (2019), who found that the most likely GMSL contribution from MICI by 2100 AD is well below 1 m (45 cm under RCP8.5), show that the probability for a GMSL rise over 1 m is not negligible. Thus, at the moment we cannot dismiss the possibility that MICI could result in a sea level rise larger than 1 m by 2100 AD, and there is not enough evidence for judging how large the weights for MICI-based projections should be. For the purposes of this study, it is therefore justifiable to go for the most pessimistic choice in cases of uncertainty (see Chapter 1).

**Table 5-1. The effect of weighting of the high-end projections of Le Bars et al. (2017) and Kopp et al. (2017) on the ASL projections at Forsmark; the ASL change from 2000 to 2100 AD (cm). Note that these values do not include the effect of isostatic uplift.**

| Weight | | 1 % | 5 % | 17 % | 50 % | 83 % | 95 % | 99 % | 99.9 % |
|---|---|---|---|---|---|---|---|---|---|
| 0 | **RCP2.6** | 11 | 15 | 19 | 30 | 43 | 54 | 73 | 119 |
| | **RCP4.5** | 18 | 23 | 29 | 42 | 57 | 70 | 93 | 133 |
| | **RCP8.5** | 29 | 37 | 46 | 63 | 83 | 111 | 155 | 219 |
| 0.25 | **RCP2.6** | 11 | 15 | 20 | 30 | 44 | 56 | 75 | 118 |
| | **RCP4.5** | 18 | 23 | 29 | 43 | 60 | 83 | 121 | 162 |
| | **RCP8.5** | 29 | 37 | 47 | 64 | 90 | 135 | 201 | 261 |
| 0.5 | **RCP2.6** | 11 | 15 | 20 | 30 | 44 | 57 | 77 | 117 |
| | **RCP4.5** | 18 | 23 | 30 | 44 | 64 | 95 | 132 | 169 |
| | **RCP8.5** | 29 | 38 | 47 | 66 | 98 | 156 | 218 | 274 |
| 0.75 | **RCP2.6** | 11 | 15 | 20 | 31 | 45 | 58 | 78 | 116 |
| | **RCP4.5** | 17 | 23 | 30 | 45 | 68 | 103 | 138 | 172 |
| | **RCP8.5** | 29 | 38 | 48 | 67 | 108 | 170 | 227 | 280 |
| 1 | **RCP2.6** | 11 | 15 | 20 | 31 | 45 | 59 | 79 | 115 |
| | **RCP4.5** | 17 | 23 | 30 | 46 | 72 | 108 | 141 | 175 |
| | **RCP8.5** | 29 | 37 | 48 | 69 | 116 | 179 | 233 | 285 |

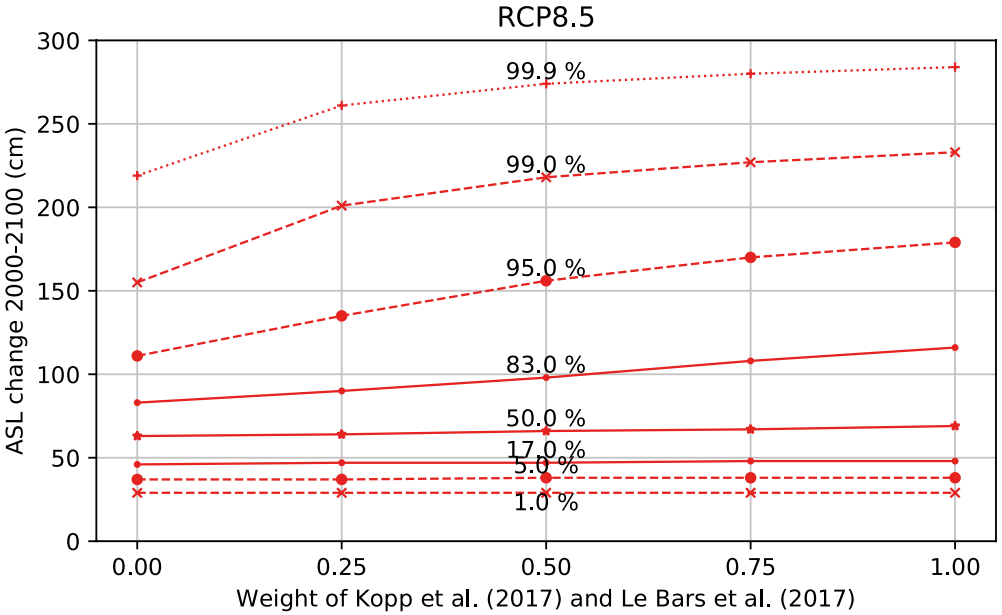


***Figure 5-1.*** *The effect of weighting of the high-end projections of Le Bars et al. (2017) and Kopp et al. (2017) on the ASL projections at Forsmark for 2100 AD, for RCP8.5. Curves for different cumulative probabilities of the ASL projection, ranging from 1 % to 99.9 % are shown.*

In this work, we choose to present the projections for the three RCPs separately, without assigning any probability to these different emission pathways. Assigning probabilities to these is a complicated task due to the deep uncertainties in the future development of technologies, policies, etc. For example Ho et al. (2019) present probabilistic judgments of experts assessing the distribution of 2100 AD emissions under a business-as-usual and a policy scenario. They conclude that there is wide variability between individual experts, but they clearly do not assign equal probabilities for the total range of future emissions. Deeper analysis of this question is beyond the scope of this study, however.

### 5.1.2 Shape of the probability distribution

When fitting probability distributions to the mean sea level projections, we test Weibull, Fréchet, and skewed Gaussian distribution functions (see Section 2.3). As previously mentioned, it turns out that none of the distribution functions gives a good fit to all projections (see also Appendix 1). The effect of the choice of fitting function is largest in the high-end tail of the distribution: at the probability level of 99.9 % the largest differences between the fitted distribution functions are approximately 20–30 cm depending on the RCP emission scenario, with the Fréchet distribution function giving the highest values (Table 5-2).

The fitting strategy used to calculate the final results is to choose the best fit for each projection, or the most conservative fit if the best fit cannot be identified. The Fréchet distribution is chosen for most of the projections because it is the most conservative, but Weibull distribution is selected in three cases where the Fréchet distribution clearly is not a good fit to the data: Goodwin et al. (2017), Kopp et al. (2017), and Le Bars et al. (2017) (Table 2-3, Appendix 1). This lowers the result by 35 cm at the 99.9 % level compared to the most conservative all-Fréchet projection.

**Table 5-2. The effect of the shape of the probability distribution fitted to the mean sea level projections (cm). These values do not include the effect of isostatic uplift (i.e. they represent the ASL change).**

| Fit | | 1 % | 5 % | 17 % | 50 % | 83 % | 95 % | 99 % | 99.9 % |
|---|---|---|---|---|---|---|---|---|---|
| Weibull | **RCP2.6** | 10 | 14 | 20 | 32 | 47 | 61 | 82 | 117 |
| | **RCP4.5** | 16 | 23 | 32 | 47 | 74 | 108 | 141 | 173 |
| | **RCP8.5** | 28 | 37 | 50 | 71 | 117 | 178 | 232 | 284 |
| Fréchet | **RCP2.6** | 12 | 15 | 20 | 31 | 43 | 56 | 77 | 118 |
| | **RCP4.5** | 18 | 24 | 31 | 46 | 68 | 96 | 138 | 205 |
| | **RCP8.5** | 30 | 39 | 48 | 68 | 111 | 160 | 224 | 319 |
| Skewed Gaussian | **RCP2.6** | 10 | 15 | 21 | 32 | 45 | 56 | 74 | 99 |
| | **RCP4.5** | 16 | 24 | 32 | 47 | 70 | 107 | 142 | 178 |
| | **RCP8.5** | 28 | 38 | 50 | 70 | 115 | 179 | 236 | 296 |
| Optimistic fit | **RCP2.6** | 10 | 14 | 20 | 32 | 46 | 58 | 77 | 115 |
| | **RCP4.5** | 16 | 22 | 31 | 47 | 71 | 107 | 141 | 175 |
| | **RCP8.5** | 27 | 37 | 49 | 70 | 116 | 178 | 233 | 284 |
| **Conservative fit** | **RCP2.6** | **11** | **15** | **20** | **31** | **45** | **59** | **79** | **115** |
| | **RCP4.5** | **17** | **23** | **30** | **46** | **72** | **108** | **141** | **175** |
| | **RCP8.5** | **29** | **37** | **48** | **69** | **116** | **179** | **233** | **285** |

We also test an optimistic fitting strategy, choosing the best fit for each projection or the least conservative fit if the best fit cannot be identified. It turns out that the results are nearly identical to those obtained using the conservative strategy (Table 5-2). We conclude that while the choice of the fitting function does add some uncertainty to the results, the method is reasonably robust to the choice of the probability distribution function.

## 5.2 Factors not taken into account in the study

### 5.2.1 Temporal changes in Baltic Sea water balance

The water volume in the Baltic Sea can be smaller or higher depending on the weather patterns: westerly winds tend to increase the water volume whereas northerly–easterly winds decrease it, due to the in- and outflow of water through the Danish Straits. So far, the results concerning this type of phenomena have not been very consistent in climate models. The water balance of the Baltic Sea was modelled as a part of our sea level simulations using the zonal geostrophic wind from the climate simulations (the second model component described in Section 3.1). These simulations indicate some increase (less than 20 cm) in the water balance component up to 2100 AD, but the models disagree even on the average value of the water balance. According to Johansson et al. (2014), Särkkä et al. (2017) and Pellikka et al. (2018), the wind-induced change in the water volume would raise the mean sea level on the Finnish coast only by some centimetres up to 2100 AD, the estimates ranging from −4 cm to +20 cm. Since the dominant winds are westerly, it is estimated that the changes at the Swedish coast would not at least be higher than these. The values are much smaller than the effect of the ASL rise and its uncertainties. Thus, the long-term change in the average water balance component in the sea level simulation was ignored, so that the entire 850-year simulation represents the sea level variability in 2000 AD.

### 5.2.2 Changes in short-term variability

Studies on the Finnish coast show that the short-term sea level variability has changed in the past. For instance, the annual sea level maxima have increased in the 20th century, and the shape of the probability distribution has changed significantly (Johansson et al. 2001). As this short-term variability is driven mainly by wind and air pressure, such changes likely reflect changes in the behaviour of these atmospheric phenomena.

The potential increase in wind speed (as well as changes in wind system patterns) in the future would impact the short-term variations of the sea level as well as the water balance of the Baltic Sea. The wind simulations from the climate models were used as input to the sea level model. The highest modelled sea level variations are quite evenly distributed for the time period 1950–2100 AD, and there is no clear indication in the model data that the sea levels variations would increase towards 2100 AD.

It is still questionable whether the climate models are able to reliably project changes in such short-term atmospheric variations. Thus, we assume that the short-term variability will be similar in the future compared to the present day, even if the observations show that changes have occurred in the past.

### 5.2.3 Wind-generated waves

The flood levels on a coastline open to waves are also affected by the wave run-up, which raises water above the still water level. Ideally, the flood probability distributions for the coastline should be calculated as a probability distribution of the sum of sea level (still water level) and wave run-up, like e.g. was done in Leijala et al. (2018). For such analysis, detailed knowledge on the local wave conditions would be needed.

The results reported here are thus applicable only to places where the still water level alone determines the flooding level. A separate study about the wave conditions is needed if waves are expected in the location of interest.

### 5.2.4 Meteotsunamis and tornadoes

Meteotsunamis (Swedish: *sjösprång*, German: *Seebär*) are sudden sea level changes of short duration, caused by a small air pressure disturbance moving above the sea. When the velocity of the disturbance matches the velocity $c$ of a long, shallow water wave ($c = \sqrt{gh}$ where $h$ is the water depth and $g$ the acceleration of gravity), the initially small wave is amplified through Proudman resonance (Proudman 1929). In the Baltic Sea, the occurrence of these waves is connected to thunderstorms and therefore they predominantly occur during the summer months. The frequency and the potential destructive power of these waves in the Baltic Sea are still poorly known. In recent years, observations of meteotsunamis

have been made at least in Finland (Pellikka et al. 2014), Sweden, and Germany. Strongest reliably documented Baltic events have reached a height of 1–1.5 m, but historical records of even higher waves exist in the literature (Doss 1906, Piotrowski et al. 2017).

Baltic meteotsunamis were reported in the literature in the 19th century and early 20th century (e.g. Doss 1906, Renqvist 1926). Since then they were more or less forgotten until recent years and have not been included in previous studies of Baltic sea level extremes. It is possible that meteotsunamis could have influenced the statistics of the extreme sea level in Forsmark, but this cannot be confirmed before comprehensive studies are made on this subject. Meteotsunamis might not be completely missing from our statistics, but they are likely to be represented with a very high uncertainty. If a meteotsunami arrives to the Öregrundsgrepen bay (Figure 1-1), it can potentially be amplified by the geometry of the bay. The height of the meteotsunami would be largest at the Öregrund town at the end of the bay and less amplified at the Forsmark repository site. Meteotsunamis occur mostly during the summer, when the water volume of the Baltic Sea is often low. This lowers the probability that a meteotsunami would coincide with high water level.

Tornadoes have a potentially large damaging impact because of their very high wind speed. In addition to the wind speed, a large and rapid change in air pressure can further enhance the damaging effects of tornadoes. The drop of air pressure in a tornado can be as large as 100 hPa. In theory, this high pressure difference could raise the water level by 100 cm. However, the time interval of a tornado passing a location is short, and the phenomenon itself has a small impact area. Rauhala (2009) estimated that the probability of a tornado hit in Finland would be of the order of $10^{-6}$ per year. The probability of a tornado hitting the site simultaneously with a high meteotsunami is extremely low, even though the mechanism that generates the tornado is in principle capable of generating a meteotsunami. This is because several other factors in addition to the steep pressure jump have to be suitable before a high meteotsunami can hit the area. If a tornado arrives over water (as a water sprout) to a site located at the shore, it can carry water with it and cause damage. There are still many unknown questions related to the frequency of occurrence, intensity, impact area, and side effects (e.g. rise of water level) of tornadoes, and the discussion on the importance and impacts of these phenomena unfortunately remains largely on a speculative level.

## 5.3 Discussion of results

### 5.3.1 Mean sea level projections

In the RCP2.6 emission scenario, the relative mean sea level at Forsmark is projected to decline up to 2100 AD, with only the most extreme tail of the distribution (the 99 % and 99.9 % levels) projecting a rise. Even the RCP4.5 emission scenario projects a decrease in the most likely projections, with only the high tail projecting some increase. In the RCP8.5 emission scenario, the median (50 %) projects practically that the relative mean sea level will first decline and then rise back to the current level by 2100 AD, while the higher end of the probability distribution projects a rising relative sea level, up to 217 cm at the 99.9 % level by 2100 AD (Table 2-5).

The extreme tail of the probability distribution has very large uncertainties, however. This is demonstrated by the analyses on the effect of weighting on the results (Section 5.1.1), which show that including or excluding high-end projections from the ensemble results in several tens of centimeters of difference in the 99 % and 99.9 % levels of the probability distribution. This reflects the deep scientific uncertainty regarding the possible worst outcomes of sea level rise over this century.

When calculating projections for the Finnish coast, Pellikka et al. (2018) included the probability range of 5 % to 95 % in their results. The results of the present study for Forsmark can be compared to those of Pellikka et al. (2018) for Föglö in the Archipelago Sea. The isostatic uplift at Föglö amounts to +6.5 mm/year, which is close to the rate of +6.7 mm/year at Forsmark.

In their study, Pellikka et al. (2018) incorporated all emission pathways in the same probability distribution. According to their analysis, the 5 % to 95 % range of RSL change at Föglö from 2000 to 2100 AD was −39 to +61 cm. At Forsmark, the corresponding ranges are −53 to −8 cm for RCP2.6, −44 to +41 cm for RCP4.5 and −29 to +111 cm for RCP8.5. There are methodological differences

between Pellikka et al. (2018) and this study, so the results are not directly comparable. However, the main reason for a considerably higher upper limit in this study is that the range of global projections extends higher than that used in Pellikka et al. (2018), where the highest projection (from Pfeffer et al. 2008) was +201 cm of global mean sea level rise by 2100 AD. More recent literature with higher projections are used in this study compared to Pellikka et al. (2018) (+243 cm from Kopp et al. 2017; +292 cm from Le Bars et al. 2017; see Section 5.1.1. for discussion on these projections). Because of the overall aim of the present study, including also the newer high-end projections is necessary.

### 5.3.2 Extreme sea levels

In Appendix 2, the exceedance frequency distributions corresponding to certain probability levels of the RSL projections (Tables 4-1 to 4-3) are plotted together with the combined distributions. The combined distributions were obtained by combining the entire probability distributions of the RSL projections with the short-term sea level variability (Tables 4-4 to 4-6) for each RCP emission scenario in 2050, 2080 and 2100 AD.

In 2050 AD, the exceedance frequencies of high sea levels obtained from the combined distributions roughly correspond to the values representing the 83 % level of the RSL projections. In the combined distributions, the high end of the RSL probability distribution thus slightly dominates. In 2080 AD, the widening of the RSL distribution, especially in the RCP8.5 emission scenario, leads to a shift of the combined distribution towards even higher RSL projections, corresponding roughly to the values representing the 95 % level. In 2100 AD, it is evident that even the shape of the combined distribution is wider than that of the distributions corresponding to certain probability levels, and the most extreme sea levels are close to those of the 99 % RSL projection.

The sea level corresponding to the exceedance frequency of $10^{-5}$ events/year is 232 cm (RH2000) in 2000 AD. The lowest of the projections in Tables 4-1 to 4-3 (RCP2.6, 50 %) projects this value to decrease to 196 cm up to 2100 AD, while the worst-case projection (RCP8.5, 99.9 %) projects a rise of more than 2 m to a value of 449 cm. The effect of the emission scenario on these values is of the order of 40–170 cm, while the RSL projection uncertainty (difference between 50 % and 99.9 % projections) is of the order of 80–220 cm. In the combined distributions (Tables 4-4 to 4-6), the effect of the emission scenario on the values corresponding to the probability of exceedance of $10^{-5}$ events/year is of the order of 20–100 cm.

As noted in Section 4.2, the behaviour of the combined distributions in 2100 AD is somewhat inconsistent in the sense that the lowest emission pathway RCP2.6 gives higher results than RCP4.5 at the low probability range. This inconsistency reflects the high uncertainties in the extreme tail (> 99.9 %) of the mean sea level distribution, where the results are based on extrapolating the probability distributions fitted to different sea level projections. Partially this inconsistency stems from the differences in projection ensembles for the different emission scenarios (Table 2-1). The ensembles of RCP2.6 and RCP4.5 consist of seven and eight projections, respectively, and the extreme tails of the distributions are dominated by one member of the ensemble, Kopp et al. (2014). The ensemble of RCP8.5, on the other hand, consists of all nine projections, and the tail is not dominated by one ensemble member. Therefore, we have higher confidence in the combined distribution of RCP8.5 in the extreme end than in the other two scenarios. However, the extrapolation of the distributions to probabilities higher than 99.9 % is inherently uncertain even in the case of RCP8.5.

The results obtained using different levels of RSL change (Section 4.1) are not affected by this extrapolation uncertainty, which only affects the MSL probability distributions in the extreme tail (> 99.9 %). For these reasons, we have lower confidence in the results obtained from the combined distributions (Section 4.2) than those obtained by assuming a certain level of RSL change (Section 4.1), especially regarding RCP2.6 and RCP4.5.

# 6 Conclusions

The exceedance frequencies of extremely high sea levels at Forsmark in 2050, 2080 and 2100 AD were calculated by combining mean sea level projections, along with uncertainties, with the short-term sea level variability (caused by wind, air pressure and seiche variations) obtained from model simulations. The following factors were not taken into account in the present study: possible future changes in short-term sea level behaviour, wind-generated waves, meteotsunamis and sea level surges induced by tornadoes.

The main conclusions of the study are:

- From 2000 to 2100 AD, the median (50 %) projection projects the mean relative sea level to decrease −36 cm in RCP2.6 and −21 cm in RCP4.5, while for RCP8.5, a rise of +2 cm is projected. Hence, except for the very end of the 21st century under the RCP8.5 scenario, the probability for a continued sea regression at Forsmark over the coming 80 years is projected to be higher than the probability for sea transgression.
- The uncertainty ranges (1 % to 99.9 %) are −57 to +48 cm for RCP2.6, −51 to +107 cm for RCP4.5, and −38 to +217 cm for RCP8.5 (Table 2-5).
- The uncertainty in the global mean sea level rise projections is reflected in the projections for Forsmark, leading into an uncertainty of 80–220 cm in the RSL projection at 2100 AD (difference between median (50 %) and 99.9 % RSL projections in Table 2-5).
- The extreme tail of the distribution is largely determined by the highest projections in the sea level rise projection ensemble, namely Kopp et al. (2017) and Le Bars et al. (2017). These two studies include high sea level rise contribution from Antarctica based on a hypothesis that is currently under scientific debate. Including or excluding these studies changes the sea level rise estimates at Forsmark by several tens of centimeters (Table 5-1). Uncertainty in the extreme tail of the distribution reflects the deep scientific uncertainty regarding the worst outcomes of sea level rise over this century. Since the aim of the study is to provide input to planning and construction of nuclear waste repositories at the coastal site of Forsmark, it is necessary to include these high-end projections even if they are highly uncertain.
- The sea level corresponding to the exceedance frequency of $10^{-5}$ events/year was 232 cm (RH2000) in 2000 AD. With the median (50 %) RSL scenario realizing, the sea level corresponding to a probability of exceedance of $10^{-5}$ events/year would be
  - 214 cm in RCP2.6, 218 cm in RCP4.5 and 224 cm in RCP8.5 in 2050,
  - 203 cm in RCP2.6, 213 cm in RCP4.5 and 228 cm in RCP8.5 in 2080, and
  - 196 cm in RCP2.6, 211 cm in RCP4.5 and 234 cm in RCP8.5 in 2100 AD (Tables 4-1, 4-2 and 4-3).
- With the high, 99 % probability level RSL scenario realizing, the sea level corresponding to a probability of exceedance of $10^{-5}$ events/year would be
  - 228 cm in RCP2.6, 243 cm in RCP4.5 and 266 cm in RCP8.5 in 2050,
  - 235 cm in RCP2.6, 275 cm in RCP4.5 and 333 cm in RCP8.5 in 2080, and
  - 244 cm in RCP2.6, 306 cm in RCP4.5 and 398 cm in RCP8.5 in 2100 AD (Tables 4-1, 4-2 and 4-3).
- With the highest, 99.9 % probability level RSL scenario realizing, the sea level corresponding to a probability of exceedance of $10^{-5}$ events/year would be
  - 237 cm in RCP2.6, 252 cm in RCP4.5 and 280 cm in RCP8.5 in 2050,
  - 258 cm in RCP2.6, 297 cm in RCP4.5 and 367 cm in RCP8.5 in 2080, and
  - 280 cm in RCP2.6, 340 cm in RCP4.5 and 449 cm in RCP8.5 in 2100 AD (Tables 4-1, 4-2 and 4-3).
- The effect of the emission scenario on these extreme sea level values is thus 10–170 cm, illustrating that future choices in emission policies have relevance for the flooding risks.

It is important to note that the results presented in the present report reflect the best scientific understanding at the moment of making the study. These types of assessments should be updated regularly in light of the most recent scientific knowledge.

**Acknowledgements**

The permission to use the 850-year sea level simulations at Forsmark site produced in a research project commissioned by Fortum Power and Heat Oy, Forsmark Kraftgrupp AB and Oskarshamn Kraftgrupp AB was kindly granted by Forsmark Kraftgrupp AB. We thank Jens-Ove Näslund and Johan Liakka, SKB, for their many constructive comments on the study and the manuscript.

# References

SKB's (Svensk Kärnbränslehantering AB) publications can be found at www.skb.com/publications.


**Bamber J L, Oppenheimer M, Kopp R E, Aspinall W P, Cooke R M, 2019.** Ice sheet contributions to future sea-level rise from structured expert judgment. Proceedings of the National Academy of Sciences 116, 11195–11200.

**Church J A, Clark P U, Cazenave A, Gregory J M, Jevrejeva S, Levermann A, Merrifield M A, Milne G A, Nerem R S, Nunn P D, Payne A J, Pfeffer W T, Stammer D, Unnikrishnan A S, 2014.** Sea level change. In Stocker T, Qin D, Plattner G-K, Tignor M, Allen S, Boschung J, Nauels A, Xia Y, Bex V, Midgley P (eds). Climate Change 2013: The physical science basis. Contribution of Working Group I to the Fifth Assessment Report of the Intergovernmental Panel on Climate Change. Cambridge: Cambridge University Press.

**Coles S, 2001.** An introduction to statistical modeling of extreme values. London: Springer.

**DeConto R M, Pollard D, 2016.** Contribution of Antarctica to past and future sea-level rise. Nature 531, 591–597.

**Dee D P, Uppala S M, Simmons A J, Berrisford P, Poli P, Kobayashi S, Andrae U, Balmaseda M A, Balsamo G, Pauer P, Bechtold P, Beljaars A C M, van de Berg L, Bidlot J, Bormann N, Delsol C, Dragani R, Fuentes M, Geer A J, Haimberger L, Healy S B, Herbach H, Hólm E V, Isaksen L, Kållberg P, Köhler M, Matricardi M, McNally A P, Monge-Sanz B M, Morcette J-J, Park B-K, Peubey C, de Rosnay P, Tavolato C, Thépaut J-N, Vitart F, 2011.** The ERA-Interim reanalysis: configuration and performance of the data assimilation system. Quarterly Journal of the Royal Meteorological Society 137, 553–597.

**Doss B, 1906.** Über ostbaltische Seebären. Gerlands Beiträge zur Geophysik 8, 367–399. (In German.)

**Edwards T L, Brandon M A, Durand G, Edwards N R, Golledge N R, Holden P B, Nias I J, Payne A J, Ritz C, Wernecke A, 2019.** Revisiting Antarctic ice loss due to marine ice-cliff instability. Nature 566, 58–73.

**Garner A J, Weiss J L, Parris A, Kopp R E, Horton R M, Overpeck J T, Horton B P, 2018.** Evolution of 21st century sea level rise projections. Earth's Future 6, 1603–1615.

**Goodwin P, Haigh I D, Rohling E J, Slangen A, 2017.** A new approach to projecting 21st century sea-level changes and extremes. Earth's Future 5, 240–253.

**Grinsted A, Jevrejeva S, Riva R E, Dahl-Jensen D, 2015.** Sea level rise projections for northern Europe under RCP8.5. Climate Research 64, 15–23.

**Hansen W, 1956.** Theorie zur Errechnung des Wasserstandes und der Strömungen in Randmeeren nebst Anwendungen. Tellus. 8, 287–300. (In German.)

**Ho E, Budescu D V, Bosetti V, van Vuuren D P, Keller K, 2019.** Not all carbon dioxide emission scenarios are equally likely: a subjective expert assessment. Climatic Change 155, 545–561.

**Holgate S J, Matthews A, Woodworth P L, Rickards L J, Tamisiea M E, Bradshaw E, Foden P E, Gordon K M, Jevrejeva S, Pugh J, 2013.** New data systems and products at the permanent service for mean sea level. Journal of Coastal Research 29, 493–504.

**Häkkinen S, 1980.** Computation of sea level variations during December 1975 and 1 to 17 September 1977 using numerical models of the Baltic Sea. Deutsche Hydrographische Zeitschrift 33,158–175.

**IPCC, 2019.** IPCC special report on the ocean and cryosphere in a changing climate [Pörtner H-O, Roberts D C, Masson-Delmotte V, Zhai P, Tignor M, Poloczanska E, Mintenbeck K, Alegría A, Nicolai M, Okem A, Petzold J, Rama B, Weyer N M (eds)]. In press.

**Jevrejeva S, Moore J C, Grinsted A, 2012.** Sea level projections to AD2500 with a new generation of climate change scenarios. Global and Planetary Change 80, 14–20.

**Jevrejeva S, Grinsted A, Moore J C, 2014.** Upper limit for sea level projections by 2100. Environmental Research Letters 9. doi:10.1088/1748-9326/9/10/104008

**Johansson M, Boman H, Kahma K, Launiainen J, 2001.** Trends in sea level variability in the Baltic Sea. Boreal Environment Research 6, 159–179.

**Johansson M, Pellikka H, Kahma K, Ruosteenoja K, 2014.** Global sea level rise scenarios adapted to the Finnish coast. Journal of Marine Systems 129, 35–46.

**Johansson M M, Kahma K K, 2016.** On the statistical relationship between the geostrophic wind and sea level variations in the Baltic Sea. Boreal Environment Research 21, 25–43.

**Kopp R E, Horton R M, Little C M, Mitrovica J X, Oppenheimer M, Rasmussen D, Strauss B H, Tebaldi C, 2014.** Probabilistic 21st and 22nd century sea-level projections at a global network of tide-gauge sites. Earth's Future 2, 383–406.

**Kopp R E, Kemp A C, Bittermann K, Horton B P, Donelly J P, Gehreis W R, Hay C C, Mitrovica J X, Morrow E D, Rahmstorf S, 2016.** Temperature-driven global sea level variability in the Common Era. Proceedings of the National Academy of Sciences 113, E1434–E1441.

**Kopp R E, DeConto R M, Bader D A, Hay C C, Horton R M, Kulp S, Oppenheimer M, Pollard D, Strauss B H, 2017.** Evolving understanding of Antarctic ice-sheet physics and ambiguity in probabilistic sea-level projections. Earth's Future 5, 1217–1233.

**Le Bars D, Drijfhout S, de Vries H, 2017.** A high-end sea level rise probabilistic projection including rapid Antarctic ice sheet mass loss. Environmental Research Letters 12, 044013. doi:10.1088/1748-9326/aa6512

**Leijala U, Björkqvist J-V, Johansson M M, Pellikka H, Laakso L, Kahma K K, 2018.** Combining probability distributions of sea level variations and wave run-up to evaluate coastal flooding risks. Natural Hazards and Earth System Sciences 18, 2785–2799.

**Meehl G A, Stocker T F, Collins W D, Friedlingstein P, Gaye A T, Gregory J M, Kitoh A, Knutti R, Murphy J M, Noda A, Raper S C B, Watterson I G, Weaver A J, Zhao Z-C, 2007.** Global Climate Projections. In: Solomon S, Qin D, Manning M, Chen Z, Marquis M, Averyt K B, Tignor M, Miller H L (eds). Climate Change 2007: the physical science basis. Contribution of Working Group I to the Fourth Assessment Report of the Intergovernmental Panel of Climate Change, 2007. Cambridge: Cambridge University Press.

**Meier H E M, Broman B, Kjellström E, 2004.** Simulated sea level in past and future climates of the Baltic Sea. Climate Research 27, 59–75.

**Mengel M, Levermann A, Frieler K, Robinson A, Marzeion B, Winkelmann R, 2016.** Future sea level rise constrained by observations and long-term commitment. Proceedings of the National Academy of Sciences 113, 2597–2602.

**Mitrovica J X, Tamisiea M E, Davis J L, Milne G A, 2001.** Recent mass balance of polar ice sheets inferred from patterns of global sea-level change. Nature 409, 1026–1029.

**Pellikka H, Rauhala J, Kahma K, Stipa T, Boman H, Kangas A, 2014.** Recent observations of meteotsunamis on the Finnish coast. Natural Hazards 74, 197–215.

**Pellikka H, Leijala U, Johansson M M, Leinonen K, Kahma K K, 2018.** Future probabilities of coastal floods in Finland. Continental Shelf Research 157, 32–42.

**Pfeffer W T, Harper J T, O'Neel S, 2008.** Kinematic constraints on glacier contributions to 21st-century sea level rise. Science 321, 1340–1343.

**Piotrowski A, Szczuciński W, Sydor P, Kotrys B, Rzodkiewicz M, Krzymińska J, 2017.** Sedimentary evidence of extreme storm surge or tsunami events in the southern Baltic Sea (Rogowo area, NW Poland). Geological Quarterly 61, 973–986.

**Proudman J, 1929.** The effects on the sea of changes in atmospheric pressure. Geophysical Journal International 2, 197–209.

**PSMSL, 2019.** Obtaining tide gauge data. Available at: http://www.psmsl.org/data/obtaining/ [12 December 2019].

**Rauhala J, 2009.** Sään ääri-ilmiöt ja ydinvoimalaitokset, Trombien esiintyminen (Extreme weather and nuclear power plants). The Finnish Research Programme on Nuclear Power Plant Safety 2007–2010 (SAFIR2010/EXWE). (In Finnish.)

**Renqvist H, 1926.** Ein Seebär in Finnland. Zur Frage nach der Entstehung der Seebären. Geografiska Annaler 8, 230–236. (In German.)

**Ruosteenoja K, Vihma T, Venäläinen A, 2019.** Projected changes in European and North Atlantic seasonal wind climate derived from CMIP5 simulations. Journal of Climate 32, 6467–6490.

**Särkkä J, Kahma K K, Kämäräinen M, Johansson M M, Saku S, 2017.** Simulated extreme sea levels at Helsinki. Boreal Environment Research 22, 299–315.

**Uppala S M, Kållberg P W, Simmons A J, Andrae U, Da Costa Bechtold V, Fiorino M, Gibson J K, Haseler J, Hernandez A, Kelly G A, Li X, Onogi K, Saarinen S, Sokka N, Allan R P, Andersson E, Arpe K, Balmaseda M A, Beljaars A C M, Van De Berg L, Bidlot J, Bormann N, Caires S, Chevalier F, Dethof A, Dragosavac M, Fisher M, Fuentes M, Hagemann S, Hólm E, Hoskins B J, Isaksen L, Janssen P A E M, Jenne R, Mcnally A P, Mahfouf J-F, Morcrette J-J, Rayner N A, Saunders R W, Simon A, Sterl A, Trenberth K E, Untch A, Vasiljevic D, Viterbo P, Woollen J, 2005.** The ERA-40 re-analysis. Quarterly Journal of the Royal Meteorologial Society 131, 2961–3012.

**van der Linden P, Mitchell J (eds), 2009.** ENSEMBLES: Climate change and its impacts: summary of research and results from ENSEMBLES project. Exeter, UK: Met Office Hadley Centre.

**Vestøl O, Ågren J, Steffen H, Kierulf H, Tarasov L, 2019.** NKG2016LU: a new land uplift model for Fennoscandia and the Baltic Region. Journal of Geodesy 93, 1759–1779.

**Witting R, 1911.** Tidvattnen i Östersjön och Finska viken. Helsinki: J. Simelii Arfvingars Boktryckeriaktiebolag. ( Fennia 29:2) (In Swedish.)

# Appendix 1

Fitting probability distributions to regional sea level rise projections in our projection ensemble (Forsmark, RCP8.5). Three types of distributions are shown: Frechét, Weibull, and skew normal distributions. Dots show the data points used in the fit (sea level rise and the corresponding probability). Left panel shows the cumulative distribution functions F, right panel shows the same in logarithmic scale (log (1-F)).

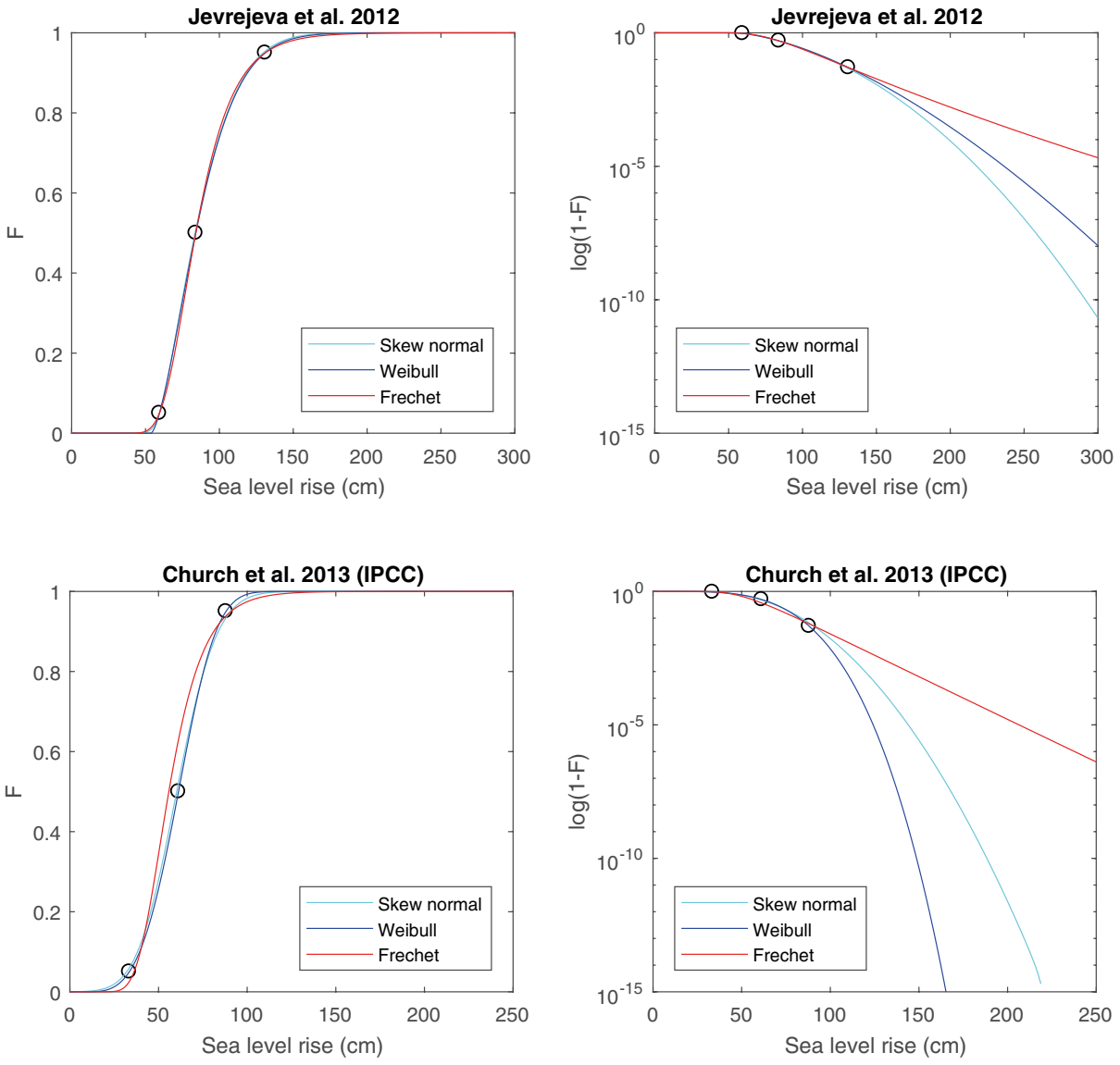

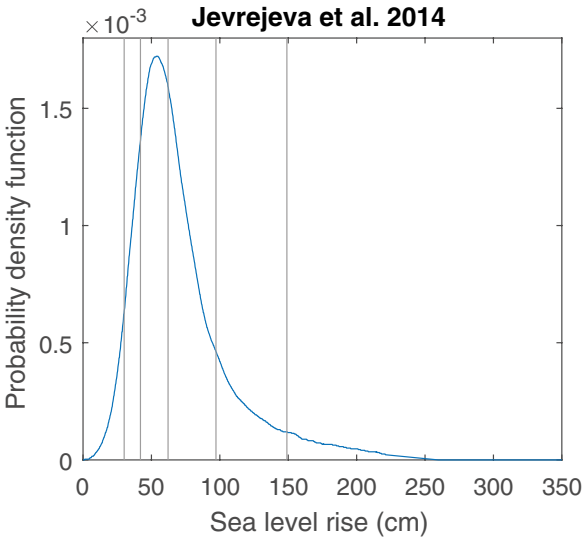
Jevrejeva et al. 2014
×10^-3
Probability density function
Sea level rise (cm)

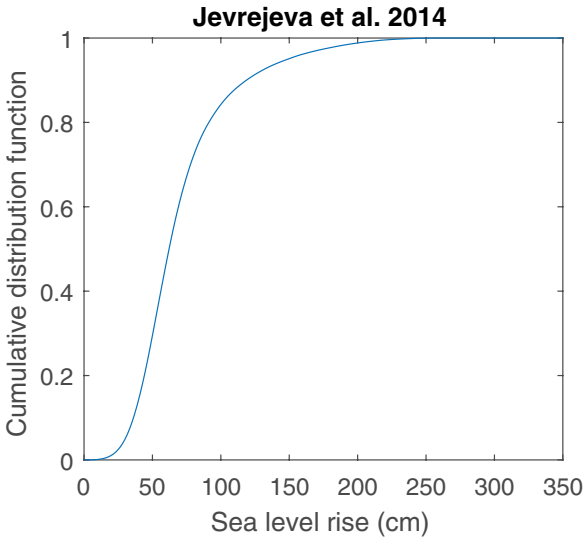
Jevrejeva et al. 2014
Cumulative distribution function
Sea level rise (cm)

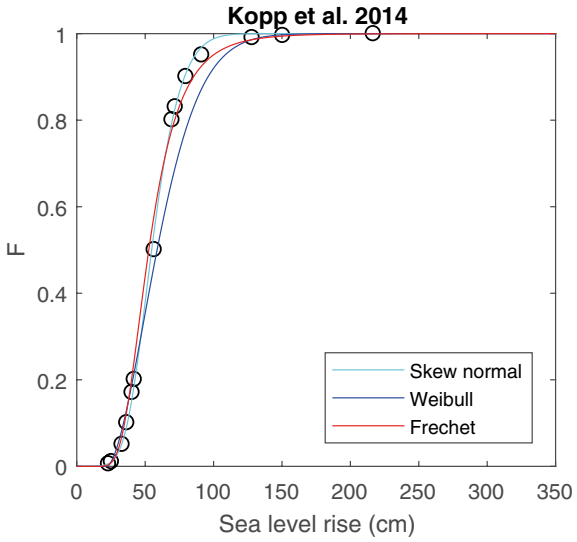
Kopp et al. 2014
F
Sea level rise (cm)
Skew normal
Weibull
Frechet

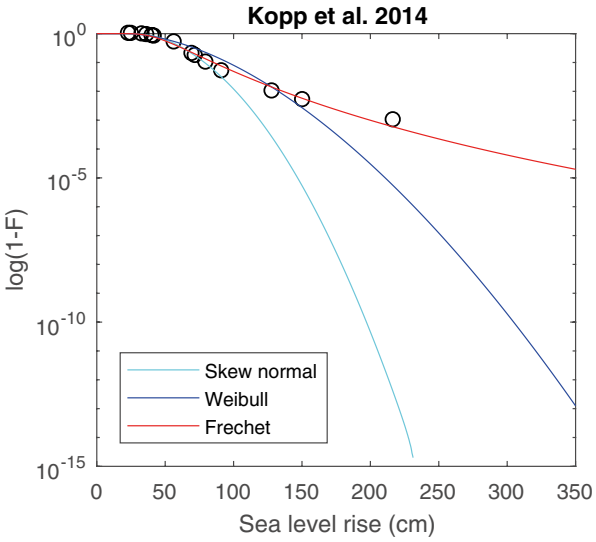
Kopp et al. 2014
log(1-F)
Sea level rise (cm)
Skew normal
Weibull
Frechet

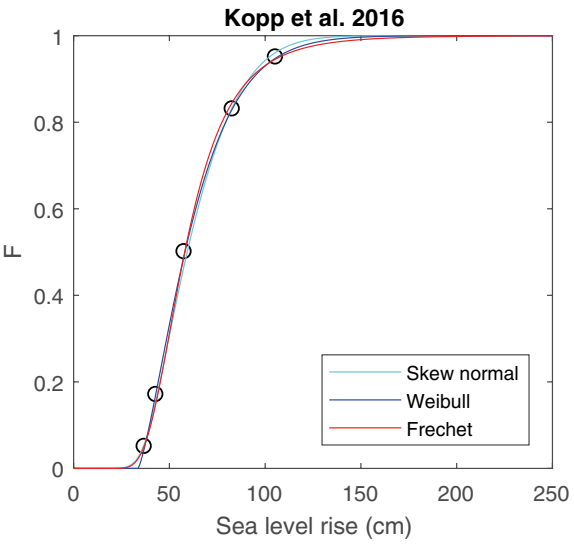
Kopp et al. 2016
F
Sea level rise (cm)
Skew normal
Weibull
Frechet

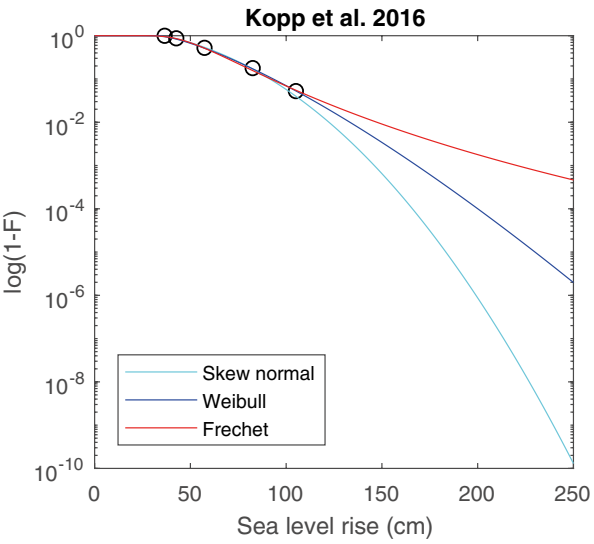
Kopp et al. 2016
log(1-F)
Sea level rise (cm)
Skew normal
Weibull
Frechet

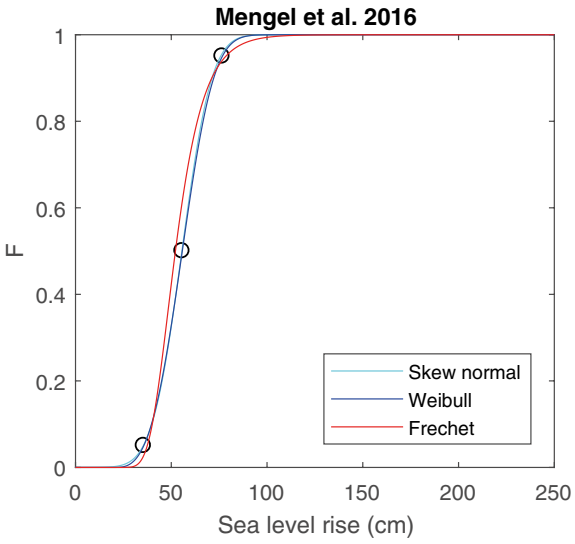
Mengel et al. 2016
F
Sea level rise (cm)
Skew normal
Weibull
Frechet

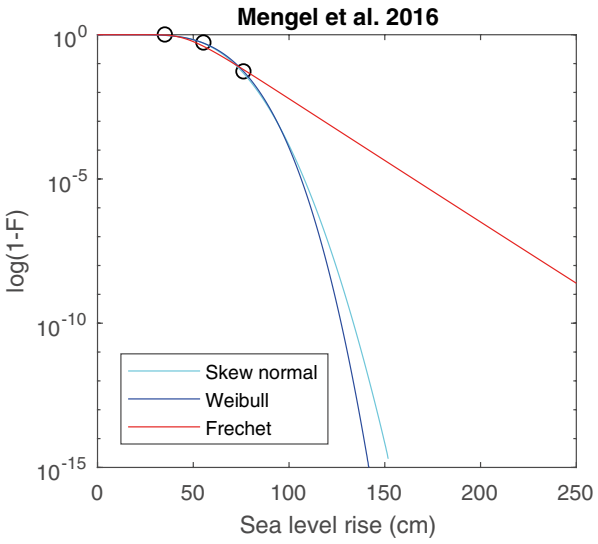
Mengel et al. 2016
log(1-F)
Sea level rise (cm)
Skew normal
Weibull
Frechet

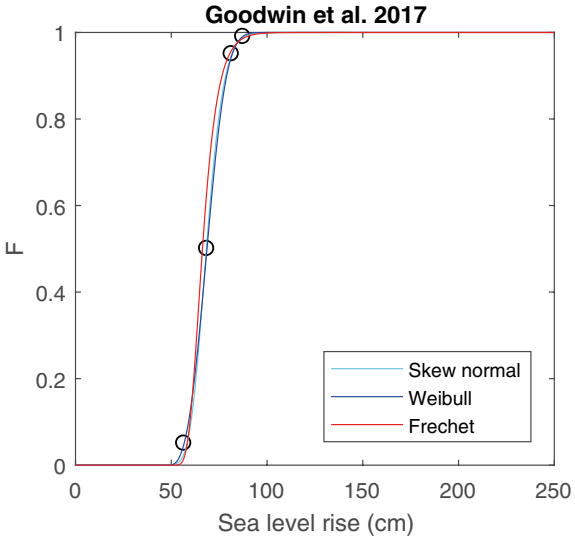
Goodwin et al. 2017
F
Sea level rise (cm)
Skew normal
Weibull
Frechet

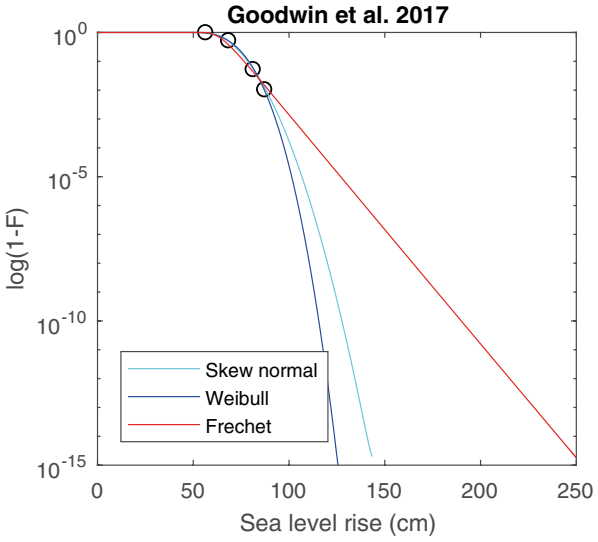
Goodwin et al. 2017
log(1-F)
Sea level rise (cm)
Skew normal
Weibull
Frechet

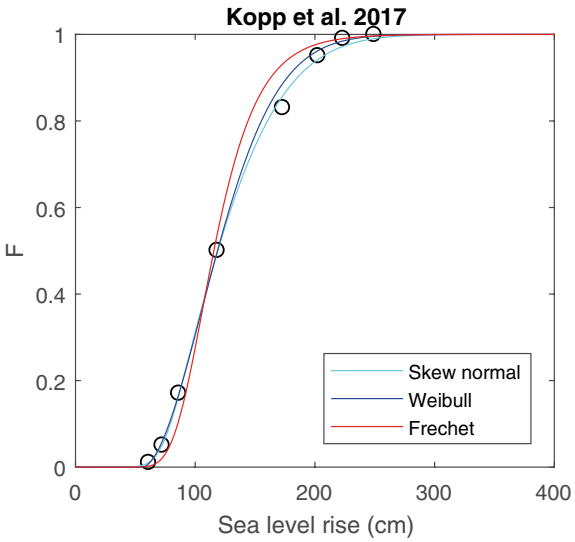
Kopp et al. 2017
F
Sea level rise (cm)
Skew normal
Weibull
Frechet

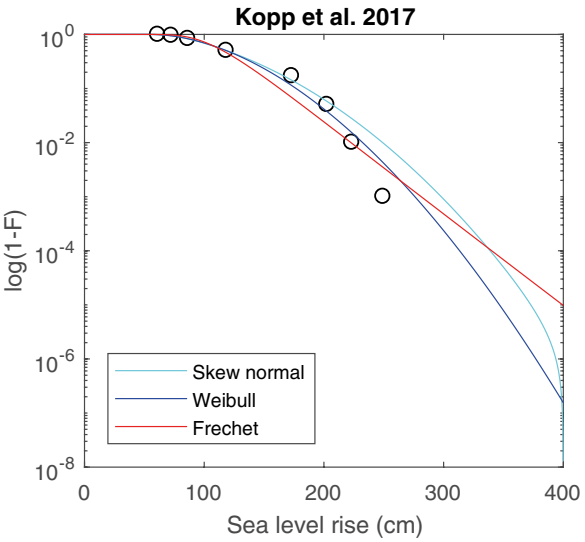
Kopp et al. 2017
log(1-F)
Sea level rise (cm)
Skew normal
Weibull
Frechet

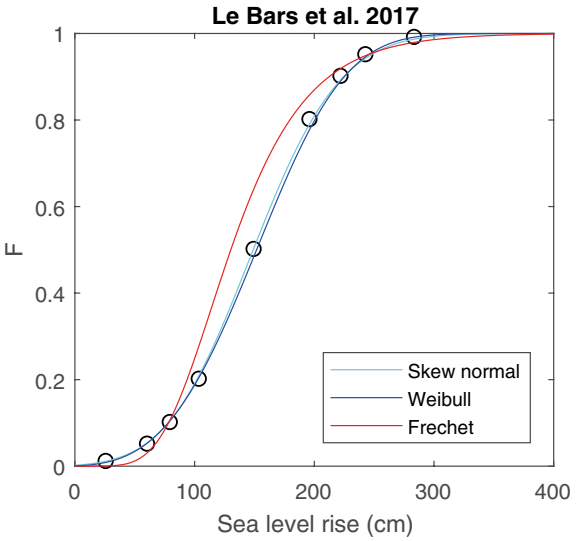
Le Bars et al. 2017
F
Sea level rise (cm)
Skew normal
Weibull
Frechet

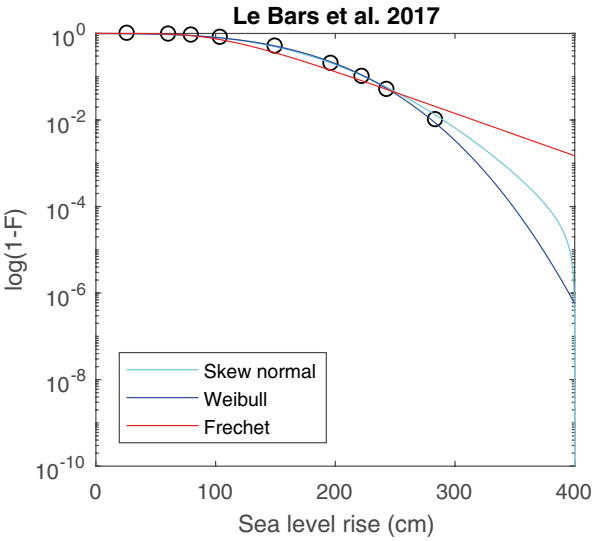
Le Bars et al. 2017
log(1-F)
Sea level rise (cm)
Skew normal
Weibull
Frechet

# Appendix 2

Sea levels (cm, RH2000) corresponding to different exceedance frequencies at Forsmark in 2050, 2080 and 2100 AD for the RCP2.6, RCP4.5 and RCP8.5 emission scenarios, assuming certain probability levels of the RSL projection (50 %, 83 %, 95 %, 99 % and 99.9 %; see Section 4.1) as well as from the combined probability distribution (see Section 4.2). These values correspond to those given in Tables 4-1 to 4-6.

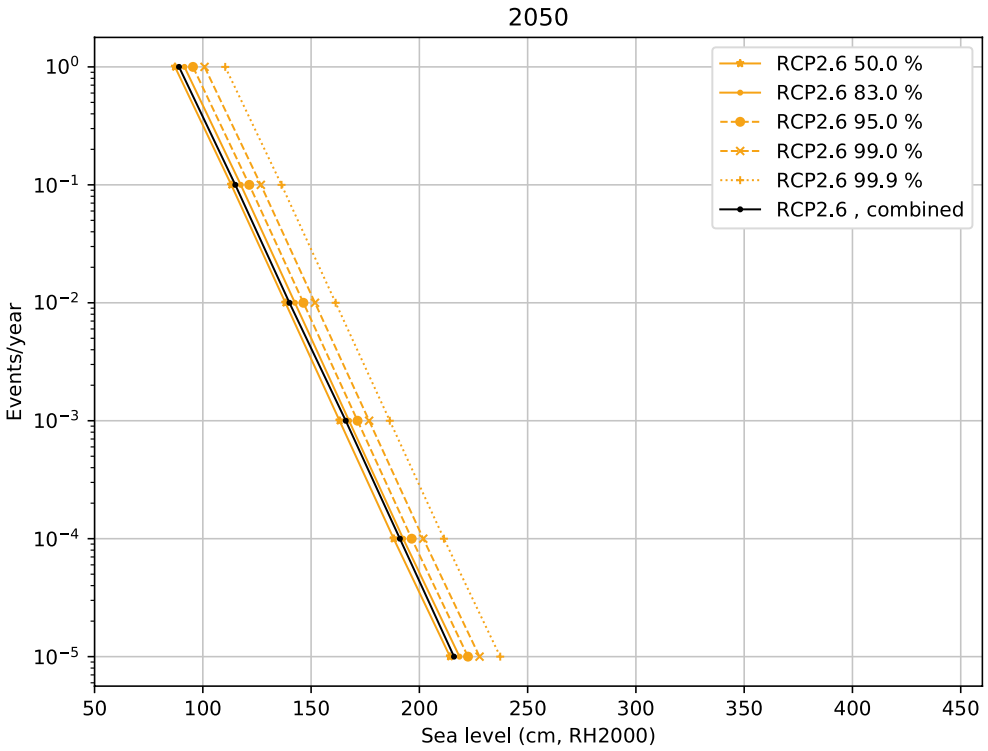


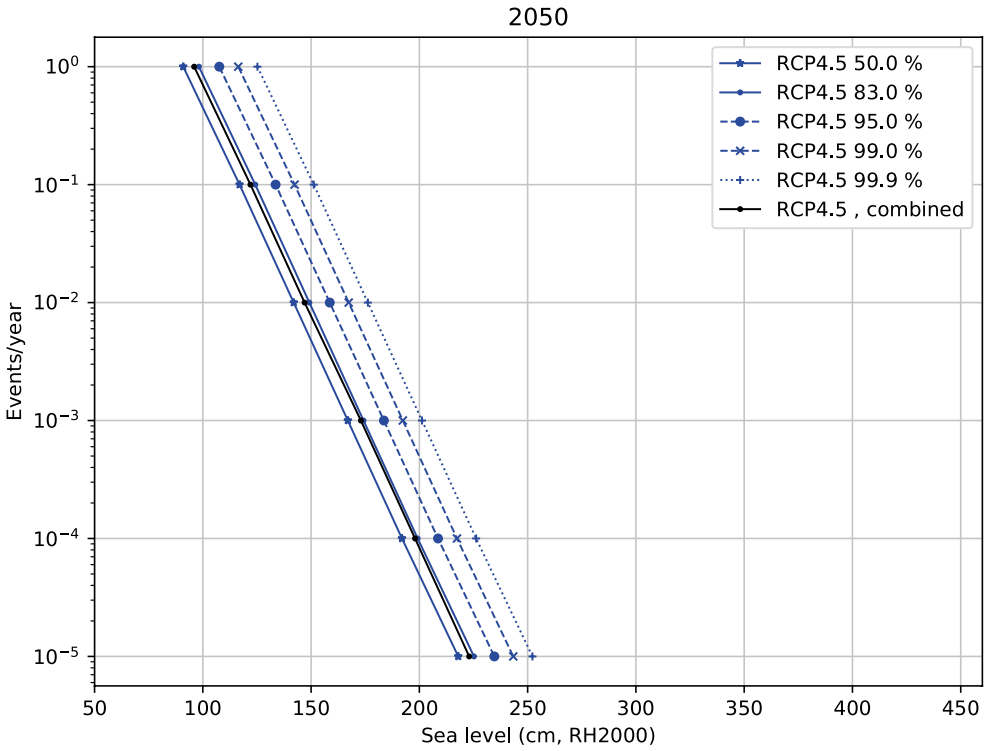

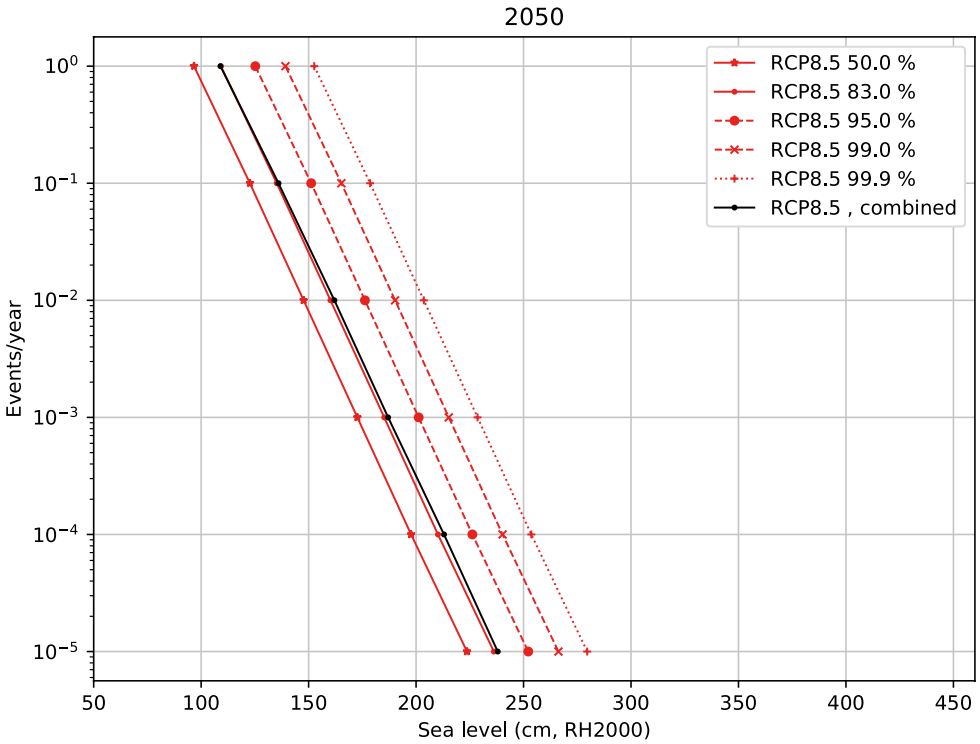
2050
RCP8.5 50.0 %
RCP8.5 83.0 %
RCP8.5 95.0 %
RCP8.5 99.0 %
RCP8.5 99.9 %
RCP8.5 , combined
Events/year
Sea level (cm, RH2000)

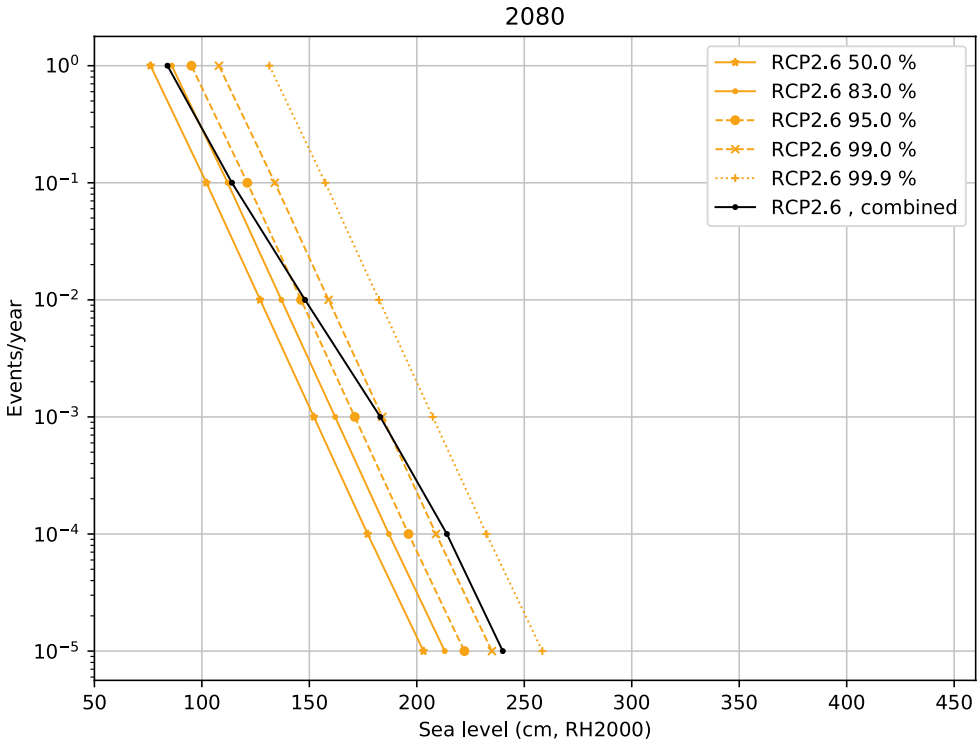
2080
RCP2.6 50.0 %
RCP2.6 83.0 %
RCP2.6 95.0 %
RCP2.6 99.0 %
RCP2.6 99.9 %
RCP2.6 , combined
Events/year
Sea level (cm, RH2000)

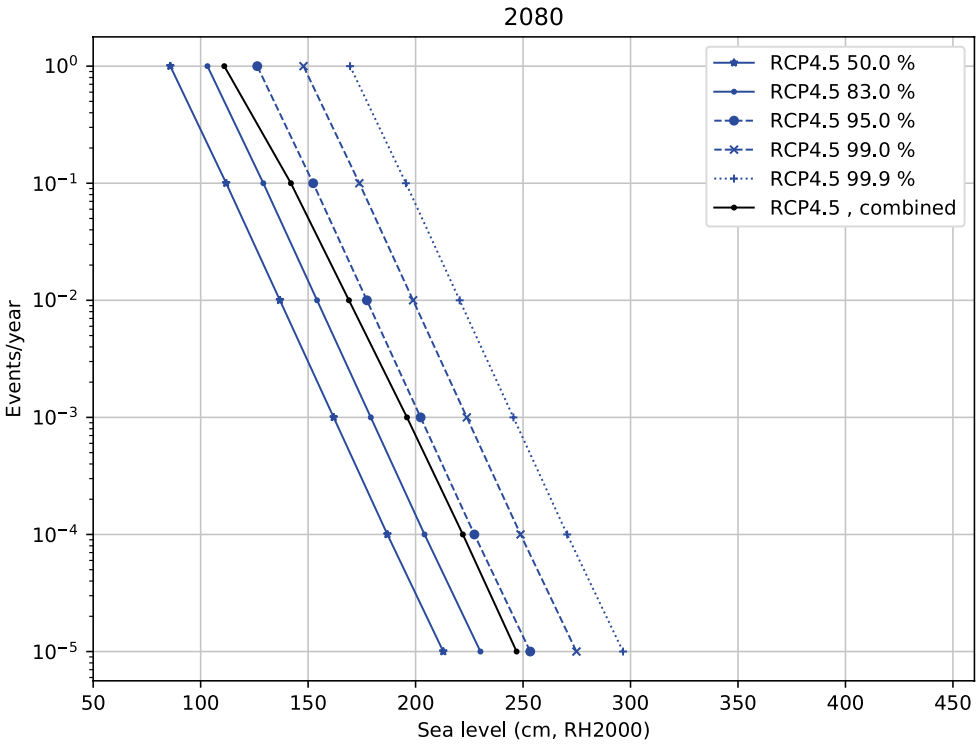
2080
RCP4.5 50.0 %
RCP4.5 83.0 %
RCP4.5 95.0 %
RCP4.5 99.0 %
RCP4.5 99.9 %
RCP4.5 , combined
Events/year
Sea level (cm, RH2000)

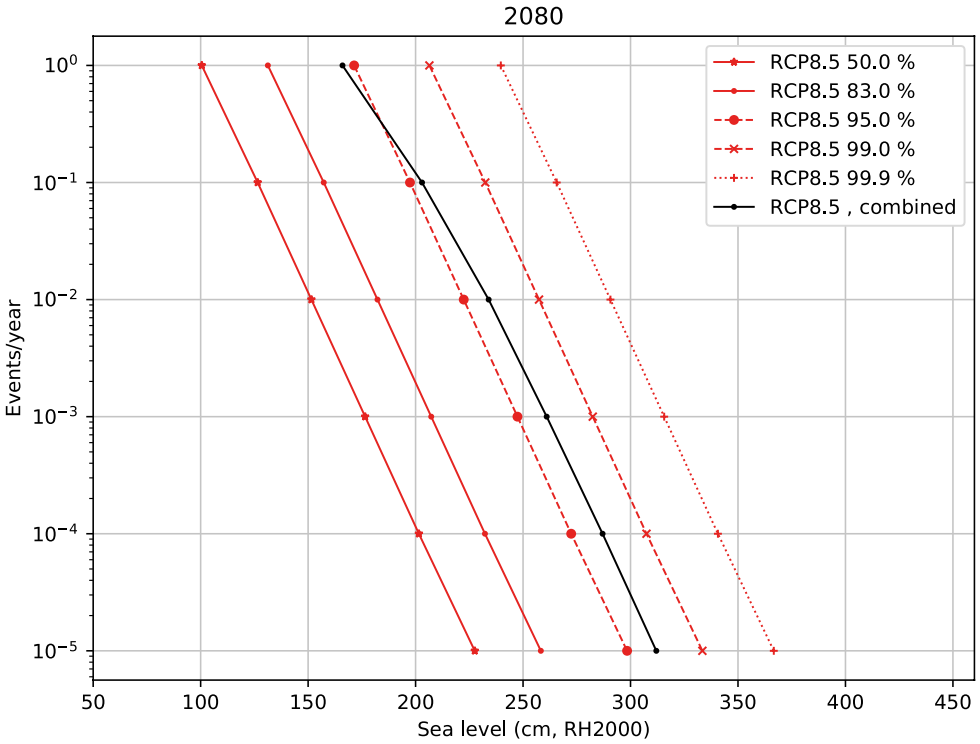
2080
RCP8.5 50.0 %
RCP8.5 83.0 %
RCP8.5 95.0 %
RCP8.5 99.0 %
RCP8.5 99.9 %
RCP8.5 , combined
Events/year
Sea level (cm, RH2000)

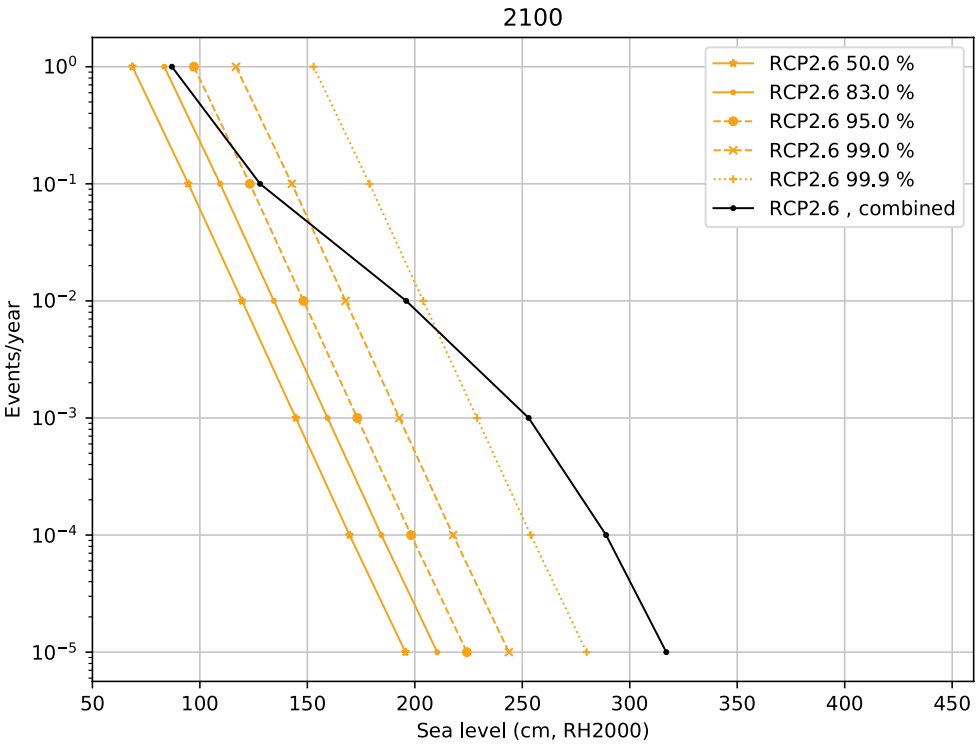
2100
RCP2.6 50.0 %
RCP2.6 83.0 %
RCP2.6 95.0 %
RCP2.6 99.0 %
RCP2.6 99.9 %
RCP2.6 , combined
Events/year
Sea level (cm, RH2000)

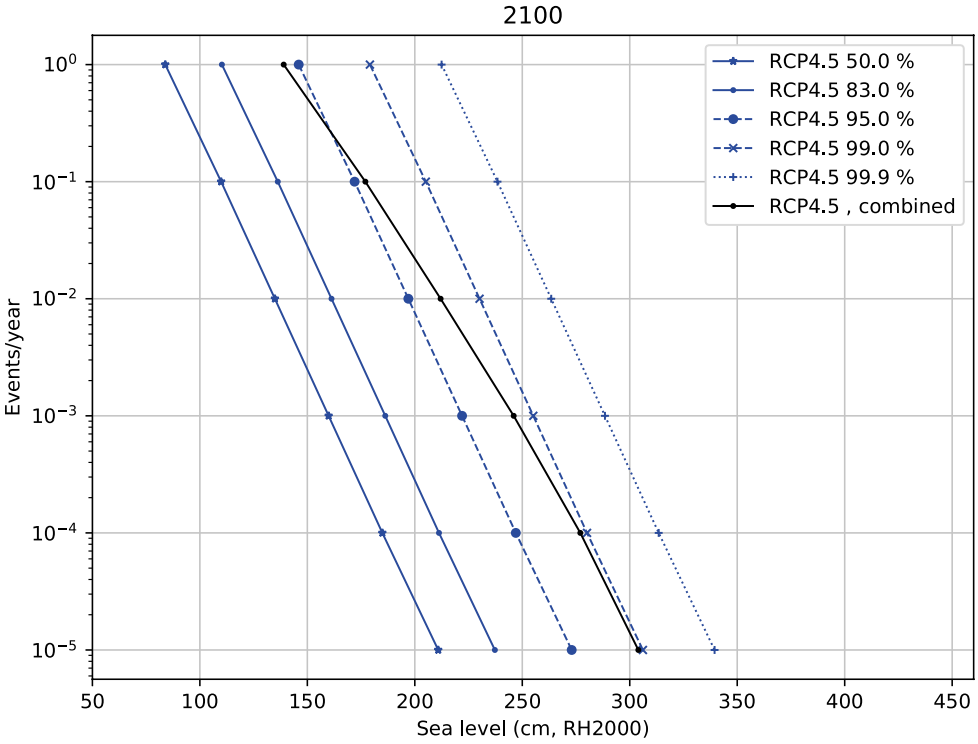
2100
RCP4.5 50.0 %
RCP4.5 83.0 %
RCP4.5 95.0 %
RCP4.5 99.0 %
RCP4.5 99.9 %
RCP4.5 , combined
Events/year
Sea level (cm, RH2000)

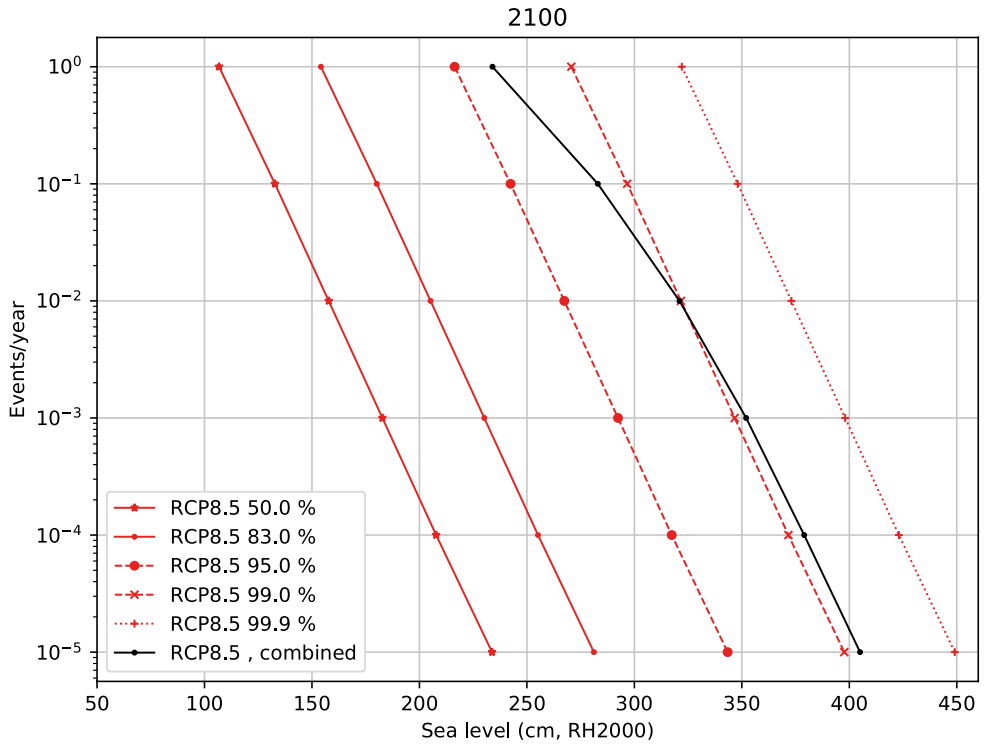
2100
Events/year
Sea level (cm, RH2000)
RCP8.5 50.0 %
RCP8.5 83.0 %
RCP8.5 95.0 %
RCP8.5 99.0 %
RCP8.5 99.9 %
RCP8.5 , combined

Arkitektkopia AB, Bromma, 2020

SKB is responsible for managing spent nuclear fuel and radioactive waste produced by the Swedish nuclear power plants such that man and the environment are protected in the near and distant future.

**skb.se**